Summer 1997

Development of a Photon Counting System for Ozone Differential Absorption Lidar Signal Detection

Bradley Allen Eccles
Old Dominion University

DEVELOPMENT OF A PHOTON COUNTING SYSTEM FOR OZONE DIFFERENTIAL ABSORPTION LIDAR SIGNAL DETECTION

by

Bradley Allen Eccles
B.S.E.E. December 1995, Old Dominion University
B.S.A.S.T.N.E.T. November 1995, Thomas Edison State College

A Thesis Submitted to the Faculty of
Old Dominion University in Partial Fulfillment of the
Requirement for the Degree of

MASTER OF SCIENCE

ELECTRICAL ENGINEERING

OLD DOMINION UNIVERSITY
August 1997

Approved by:

Hani E. Elsayed-Ali (Director)

Amin N. Dharamsi (Member)

Linda L. Vahala (Member)

ABSTRACT

DEVELOPMENT OF A PHOTON COUNTING SYSTEM FOR OZONE DIFFERENTIAL ABSORPTION LIDAR SIGNAL DETECTION.

Bradley Allen Eccles
Old Dominion University, 1997
Director: Dr. Hani E. Elsayed-Ali

A photon counting system was assembled and integrated into an existing ozone differential absorption lidar signal detection system to improve the range of ozone measurement. Results of data extraction from decaying ozone return signals are presented. Photomultiplier tube detector models EMI 9214Q and EMI 9817Q are evaluated and characterized. Detector operating performance was based on tube quantum efficiency, gain, dark current, and linearity. The influence of photomultiplier tube characteristics on photon counting performance are discussed along with the recommended optimum photon counting operating conditions. Two photomultiplier gating schemes, focus grid and four dynode gating, are described for use in photon counting systems.

ACKNOWLEDGEMENTS

I would like to begin with recognizing Dr. Amin N. Dharamsi, who first brought the Senior Thesis Option to my attention. I am indebted to Dr. Hani E. Elsayed-Ali for the opportunity to participate in this Senior Thesis Project and for his pro-student oriented philosophy. I would like to thank Dr. Linda L. Vahala for reviewing this manuscript and for being on my committee. Also, I must thank all of the members of the National Aeronautics and Space Administration Langley Research Center, Lidar Applications Group, who's support and technical insight helped me to complete this project: Dr. Russell DeYoung (for his guidance and support), Dr. Edward Browell, Arlen Carter, Carolyn Butler, Jerry Williams, Dale Richter, William McCabe, Mark Jones, Byron Meadows, and Lloyd Overbay. Most of all, I want to express my deepest appreciation to my wife, Lisa Ann Eccles, for all of her support in this endeavor and to the joy given to me by my daughter, Bree Ann Eccles.

TABLE OF CONTENTS

CHAPTER PAGE

LIST OF TABLES

LIST OF FIGURES

CHAPTER I

INTRODUCTION

1.1 Photon Counting in Atmospheric Science Measurements

Photon counting is a light signal measurement technique which utilizes the inherent discrete nature of light [1]. A light signal is comprised of individual wave packets called photons. The energy of a photon is proportional to its wavelength and is governed by the relationship $E_\gamma = h\nu$, where h is Planck's constant and ν is the frequency in Hertz. Therefore, a photon detection scheme provides the most sensitive method to measure a light signal. Implementing the photon counting measurement technique into current atmospheric measurements of ozone presents the most favorable means of extending the detection range.

A typical photon counting system consists of a photon detector, an amplifier, a pulse height discriminator, and a pulse counter [1]. When very low level light signals are measured, a photomultiplier tube (PMT) is used to detect and convert individual photons incident on the PMT into electrical pulses for photon counting measurements.

A high bandwidth, low noise amplifier is necessary to convert the low voltage, high impedance output of the PMT to the required low impedance input for the pulse height discriminator. The pulse height discriminator produces a

---

Journal model used in this thesis is Applied Optics.

fixed pulse width and height for every photon pulse detected above a certain voltage level. Thus, unwanted noise pulses are rejected improving the signal-to-noise ratio.

The photon counting technique has the ability to detect single photons. This is performed by utilizing the unique characteristics of a photomultiplier's inherent sensitivity and amplification that is able to detect single photon events over a large photocathode area [1,2]. However, as the photon detection system is exposed to higher count rates, the statistical advantage associated with photon counting becomes unsatisfactory and analog signal processing is necessary. To take advantage of the high gain offered by the PMT, the applied tube DC high voltage must be increased. The increase of high voltage leads to a corresponding increase of unwanted dark current which reduces the counting system's signal-to-noise ratio. To suppress this effect requires the incorporation of a means of signal discrimination [1,2]. Discrimination of the PMT's anode signal output offers many benefits. Output signal discrimination minimizes fluctuations of photomultiplier gain which contributes to noise in analog measurements, allows for dark current suppression with proper threshold settings, and eliminates the counting of leakage currents which occur between photomultiplier socket leads [2]. The addition of signal preamplification and discrimination adds to the overall complexity of the photon counting system.

Combine these complications along with the individual operating characteristics of PMTs of even the same model and the determination of proper system parameters becomes a detailed process. The optimum operating conditions of a photon counting system depend on the nature of the measurement. The implementation of a PMT permits the detected photon to be separately time resolved at the anode. To acquire adequate values for a particular measurement may require relatively long integration times. Increasing the system's count times must be balanced against desired photon counting sensitivity and the amount of data collected for system analysis.

1.2 Ozone Measurement and its Importance

Ozone measurement is accomplished by utilizing the differential absorption lidar (DIAL) measurement technique (lidar is an acronym for light detection and ranging). Two tunable lasers are used to transmit their respective light output into the atmosphere. Light scattered from atmospheric ozone molecules is captured by a detection system and then processed and stored by a computer-based data gathering system [3,4]. The DIAL technique will be covered in greater detail in Section 2.3.

The measurement of ozone concentrations in the upper and lower atmospheres has become increasingly important towards gaining a global understanding of the Earth's environmental processes. Ozone molecules at about 24

kilometers in the upper atmosphere, or stratosphere, act as a ultraviolet radiation protective shield for life on the Earth's surface. Ozone molecules interact with ultraviolet radiation from the sun to produce an oxygen molecule and a free oxygen atom. Ozone that is found in the air of the lower atmosphere, or troposphere, is considered a harmful pollutant which posses a hazard to lung tissues and plants and functions as a greenhouse gas component [5,6]. Long term exposure to elevated ozone levels is associated with reduced lung function (aging), intensification of asthma related symptoms, and airway cell and tissue changes [7]. The balance of ozone in the stratosphere and troposphere depends upon the processes that supply and deplete it. Towards developing an understanding of the Earth's environmental processes, measurement of ozone concentrations is necessary in order to establish an accurate data base upon which theories and public policy can be based. It is important for individuals to understand and respect their ability to influence change on a global basis and not to restrict their perception to their respective local proximity.

Since its inception in 1978, the Lidar Applications Group (LAG), at NASA Langley Research Center, has developed and applied advanced lidar systems for atmospheric investigations. The principal instrument used for atmospheric studies is the application of airborne DIAL

systems for the analysis of ozone, water vapor, aerosols, and clouds. In 1980, the LAG made the first remote ozone and aerosol profile measurements using an airborne DIAL system. In 1981, the first troposphere water vapor profiles were obtained. International field experiments began in 1982 over the tropical Atlantic from Puerto Rico and have continued over diverse terrains in selected seasonal conditions. In the past thirteen years, airborne DIAL systems have conducted ozone and aerosol measurements in conjunction with NASA's Global Tropospheric Experiments (GTE), which study the role of tropospheric chemistry in regards to global change.

The 1990 Clean Air Act Amendments, which mandate compliance with near-surface ozone standards established by the Environmental Protection Agency, have generated an international effort striving to develop and implement various atmospheric ozone measurement designs [8]. Examples of ozone atmospheric studies include small-sized airborne lidar experiments and continuous operational lidar stations located in extreme environmental conditions such as Norway, Japan, Canada, Germany, and the United States of America [8-12]. These diverse international research efforts are concentrating upon ozone distributions and chemical dynamics occurring in the troposphere and stratosphere atmospheric regions. Lidar measurements utilize the ultraviolet spectrum produced by various combinations of excimer,

Nd:YAG, and dye lasers. Common to all of these detection schemes is the incorporation of a photon counting system. Photon counting has been the suggested method in order to increase the measurement range of atmospheric studies [8-12].

1.3 Goal of This Research Effort

Photon counting has been chosen as a means to extend the detection range of current airborne DIAL ozone measurements. Lidar backscattered return signals from the on and off-line lasers experience a significant exponential decay. To extract further data from the decaying ozone return signals, photon counting will be used to measure the low light levels, thus extending the detection range. In this application, photon counting will extend signal measurement where the analog return signal is too weak.

The current analog measurement range is limited to approximately 25 kilometers from an aircraft flying at 12 kilometers as exhibited in Figure 1.1 [13]. Photon counting will be used to exceed the current measurement range in order to follow the Mid-latitude model of ozone density as a function of height as is shown in Figure 1.2 [14].

This thesis describes the development of a photon counting system. The initial development phase begins with detailed evaluation of individual photomultiplier tubes. The PMT qualities investigated are noise count rates, single electron response peaks, voltage versus gain values,

saturation effects, and output signal linearity. These evaluations are followed by analysis of two distinctive tube base gating schemes. The next phase is to construct and operate a photon counting system in a laboratory environment. The laboratory counting simulations are used to determine optimum discriminator setpoints and to continue further evaluations of PMT properties. The final step in the photon counting system evaluation process is the compiling of photon counting measurements on the existing ozone DIAL laser system.

In this thesis, the objectives outlined below describes the development of a photon counting system that is to be utilized in a ozone DIAL signal detection system. The investigation are discussed in three chapters. Theoretical analysis of photon counting and the DIAL equation are introduced in Chapter II. This chapter discusses photomultiplier operation and its application in a differential lidar photon counting system. Next, in Chapter III, the photon counting system components are presented and discussed, along with the analysis equipment employed and tube base gate designs. Finally, in Chapter IV, the experimental results in the laboratory and field demonstrate the expanded ozone detection range offered by the addition of the photon counting system in the differential lidar signal process. Chapter V summarizes the important

conclusions of this work and applicability to ozone detection.

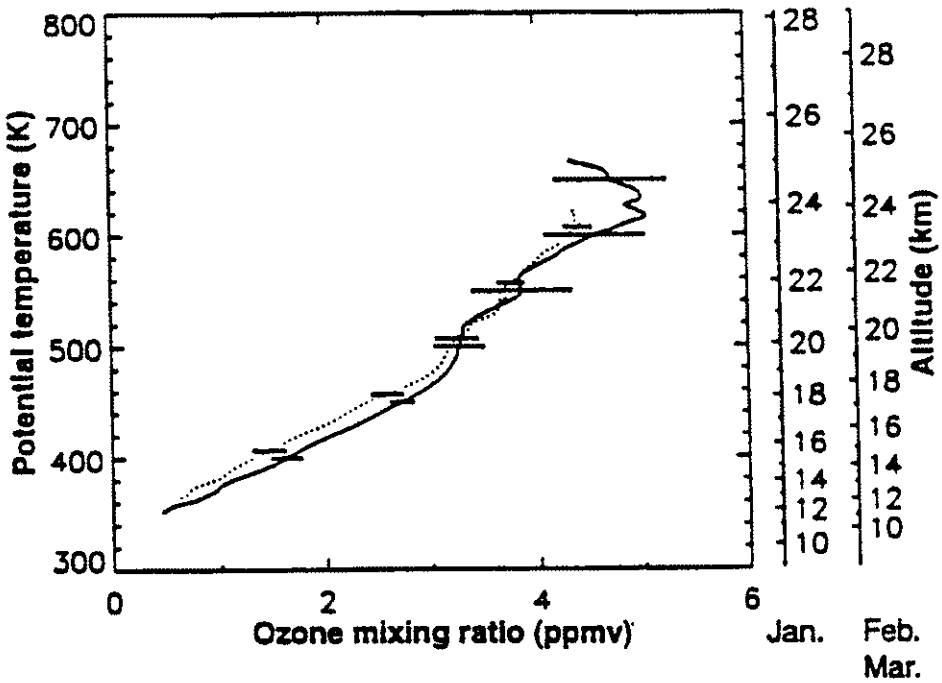

Figure 1.1. Comparison of average ozone profiles for January (solid line) and February (dotted line) 1992 [13].

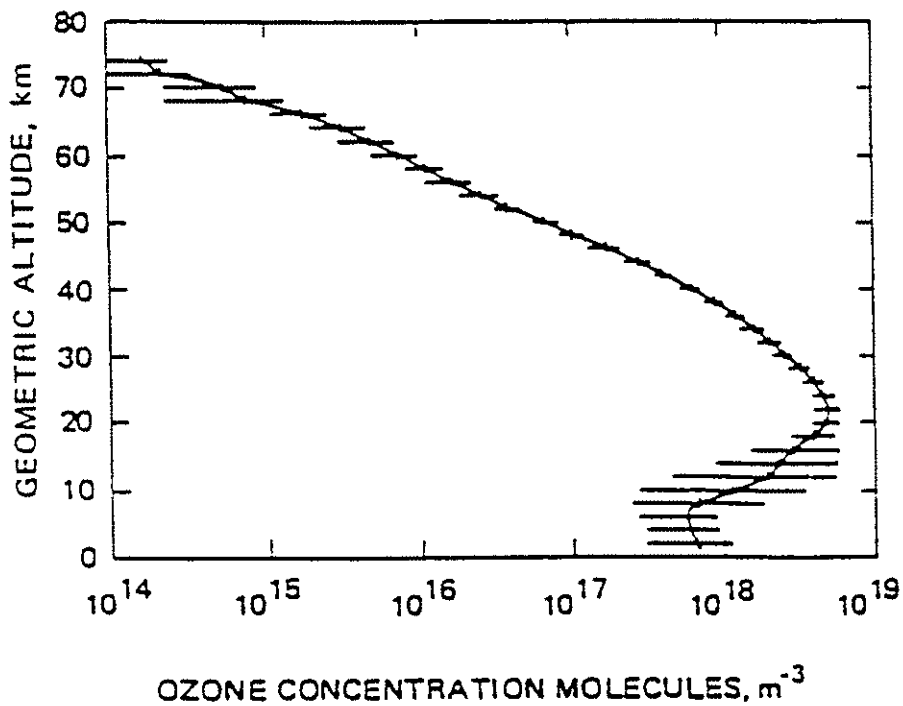

Figure 1.2. Mid-latitude model of ozone density as a function of height [14].

CHAPTER II

THEORY

The development of a photon counting system requires an understanding of the theoretical operation of the detector and associated components. This Chapter will begin with a discussion of photomultiplier tube operation characteristics and the concept of photon counting. Paralyzable and nonparalyzable photon counting system classification will also be discussed. A brief introduction to the DIAL equation is given, along with an explanation of associated system errors. Finally discussion will consider the application of photon counting in a lidar based measurement of stratospheric ozone.

2.1 Theory of Photomultiplier Tube Operation

A photomultiplier tube (PMT) is a device used for detection of very low energy light signals. A PMT consists of three main elements: a photocathode, dynodes, and an anode [1,15]. The photocathode converts incident light into photoelectrons that are emitted into a vacuum. The photoelectrons are guided by a focusing electrode to a twelve stage dynode chain where electron amplification takes place. The dynodes emit other electrons, creating a swarm of electrons at the end of the dynode chain. The dynode chain can easily have a gain of 10^6 to 10^8 depending upon the applied voltage. At the end of the dynode chain, the

electrons strike the anode plate creating an electrical pulse. The current pulse flows through a 50 ohm load in the external circuit where a voltage signal is observed.

The choice of a photomultiplier tube depends upon the desired application and performance characteristics of the individual tube. The PMT's used for photon counting and system verification are listed in Chapter IV. Main characteristics to consider when choosing a tube for a given wavelength are photocathode quantum efficiency, gain, dark current, linearity, and speed of response. Optimization of these characteristics results in maximizing a photomultiplier's signal-to-noise ratio (SNR).

Quantum efficiency describes the average number of electrons emitted from the photocathode per incident photon of a given wavelength. The photoelectron current produced by the photocathode is directly related to the number of incident photons and the quanta of energy necessary to release an electron from a surface. The emission of a photoelectron can be considered as a series of three steps: 1) absorption of a photon, with a transfer of energy from the photon to an electron, 2) movement of the excited electron towards its material-vacuum interface, and 3) escape of the electron from the energy potential barrier at the material-vacuum interface [1,15]. There are energy losses during each of these steps. Any energy loss during these steps lead to a reduction in the overall quantum

efficiency of the photomultiplier. Operating characteristics directly related to a photomultiplier's quantum efficiency are its resolution potential and signal-to-noise. Typical peak quantum efficiencies range from 10-35% in the ultraviolet region of the spectrum. The highest possible quantum efficiency is desired at the operating wavelength for the best signal-to-noise response. Determination of quantum efficiency versus incident wavelength is necessary for photon counting system optimization. The quantum efficiencies of three EMI 9214Q PMTs are shown in Figure 2.1 over a 250 to 350 nanometer range (evaluation of PMT quantum efficiencies were performed by Burle Industries). The distribution of quantum efficiency values requires the need for individual PMT evaluation under the desired operating conditions.

Gain of a PMT describes the ratio of output (anode) signal current to photoelectron current emitted by the photocathode. Gain values may range from 10^3 to 10^8 in a linear relationship such as that shown in Figure 2.2 (evaluation of PMT current gains were performed by Burle Industries) [15,16]. Generally, tube selection is based upon the highest gain possible at the operating wavelength. The range of gain is controlled by the applied voltage which allows adjustable gain operation. A voltage divider network is necessary to distribute the high voltage DC power supply to each dynode interstage for amplification by secondary

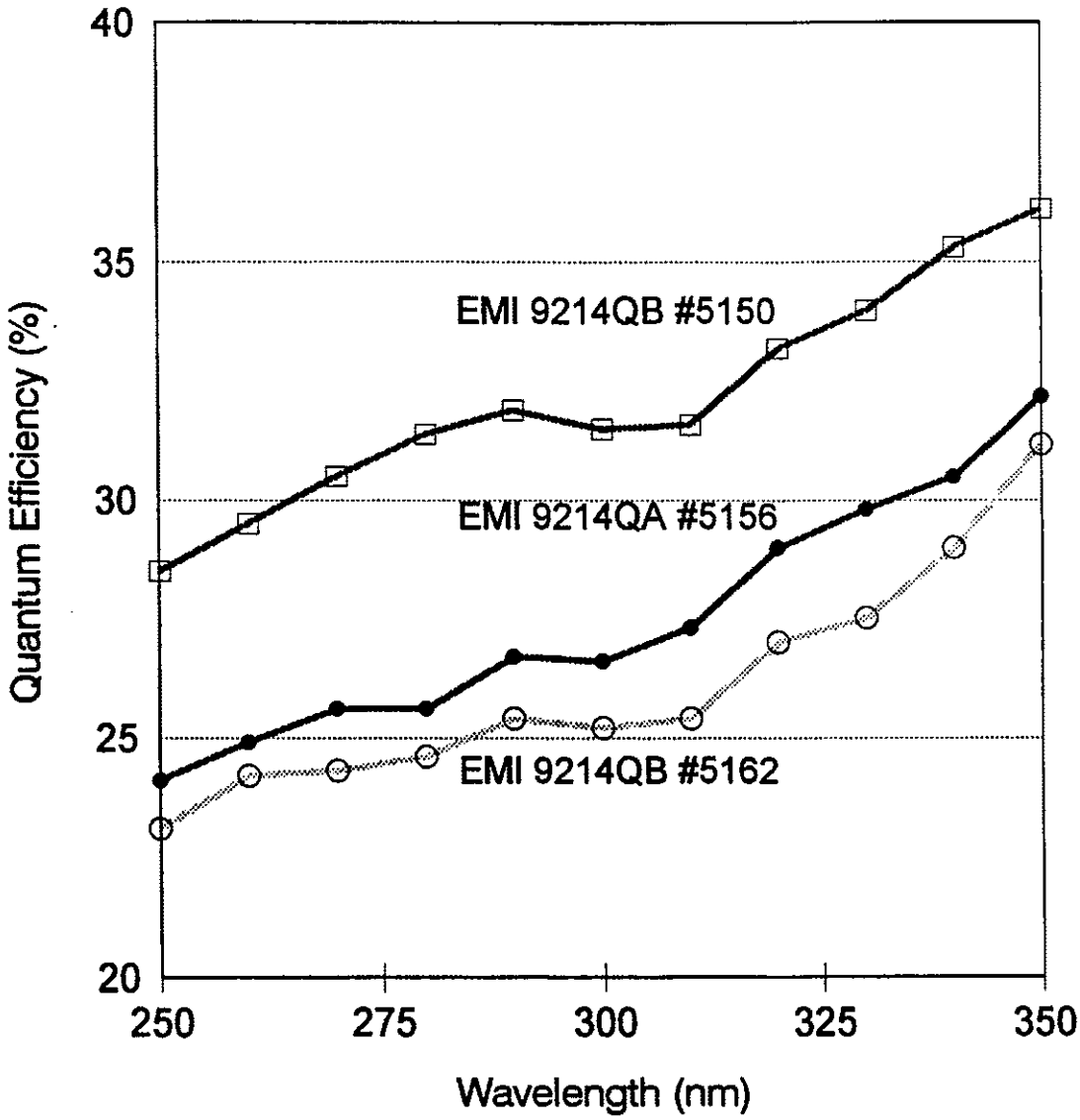

Figure 2.1. Data plots of quantum efficiency versus wavelength for three EMI 9214Q series [evaluation performed by Burle Industries].

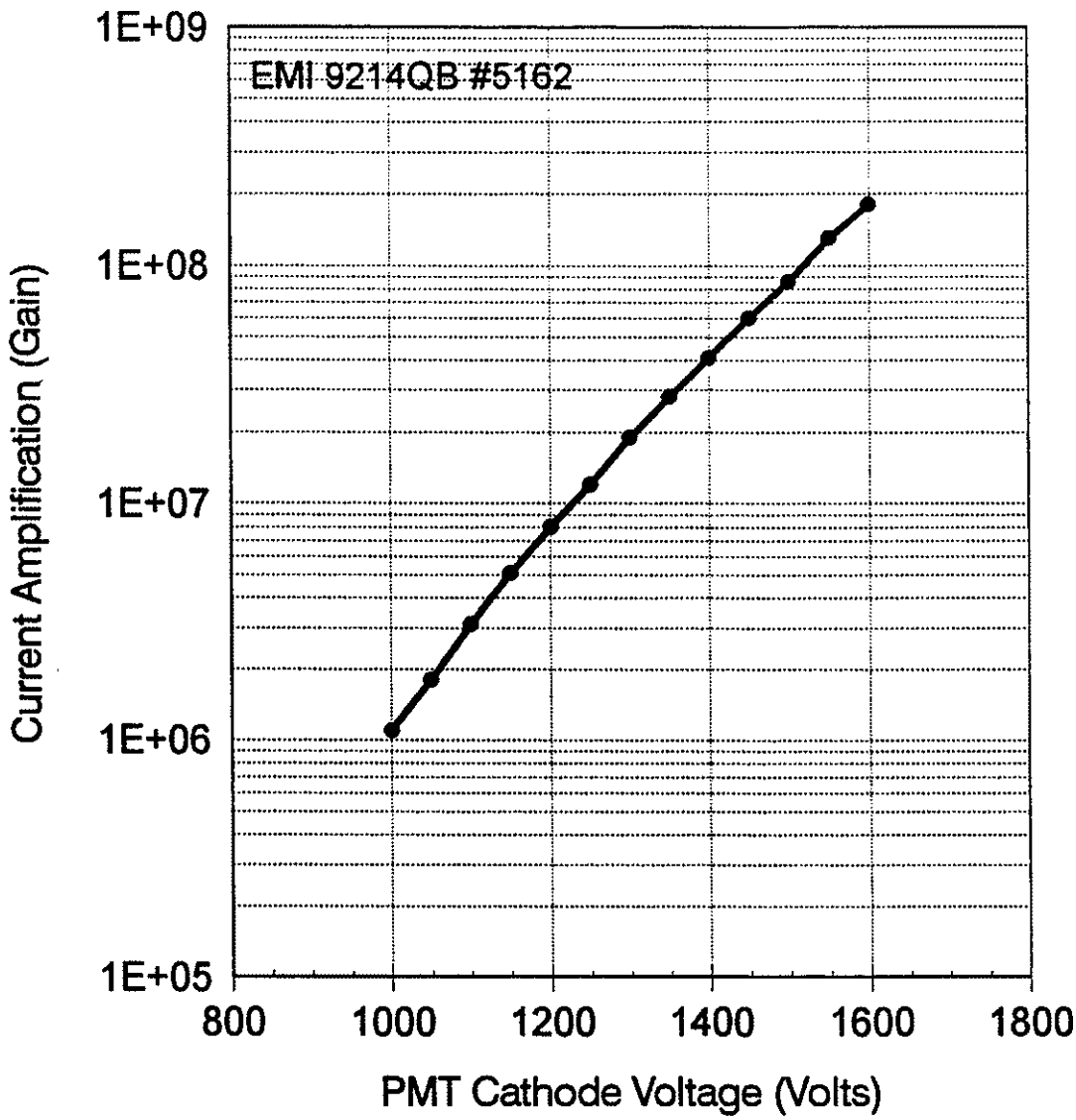

Figure 2.2. A sample photomultiplier gain curve [evaluation performed by Burle Industries].

electron emission. Voltage divider network design is discussed in further detail in Section 3.3.

A PMT is subject to unwanted emissions that place a lower limit on the light level sensitivity of the device. Dark current and statistical pulse fluctuations influence PMT performance [1,15]. Photomultiplier dark current is a small DC current that is generated in the absence of light. The source of gain-proportional, dark current is attributed to thermionic emission which is photoelectron emissions produced by the dynodes and photocathode that are not the result of photons incident upon the photocathode. Values of dark current are typically in the nanoampere region and the lowest possible dark current is used for PMT selection. Dark current is very temperature sensitive and also dependent upon the photocathode material. Statistical noise fluctuations are due to photoelectron noise produced from within the PMT. Electrons that are not generated by the photocathode but are emitted by different dynode stage surfaces have lower peak output voltages. The noise pulses are lower than the photoelectron pulses due to the fact that noise pulses only travel through part of the dynode chain. Figure 2.3 shows an example of a tube's signal rate, dark count rate (dark current), and signal-to-noise ratio. It can be seen that as the applied PMT cathode voltage is increased, associated increases in output signal and dark current occur as well. However, as the cathode voltage

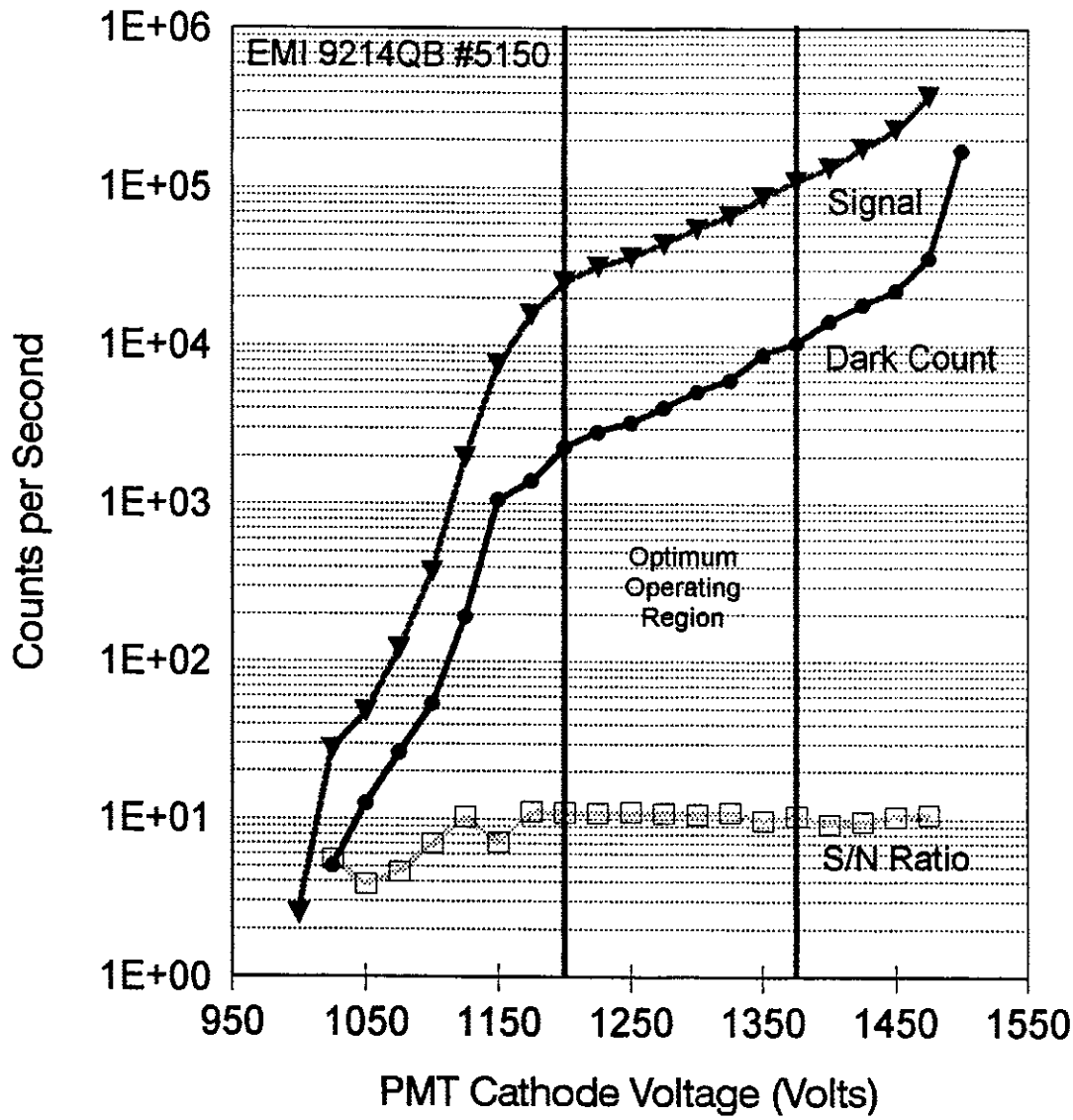

Figure 2.3. Plots of a photomultiplier tube's signal rate, dark count rate, and signal-to-noise ratios are used in finding the optimum operating voltage for photon counting.

continues to advance, the slope of the dark current begins to surpass that of the PMT's signal. This leads to lowering of the tube's signal-to-noise ratio. The use of this figure allows the determination of the optimum operating voltage for photon counting. Tube optimization begins by identifying the signal plateau region. An operating point on this signal plateau that maximizes the signal-to-noise ratio while minimizing the dark counts regularly provides for acceptable PMT performance [15,16].

Photomultiplier linearity describes the relationship between the magnitude of incident light to anode current output. Linearity involves two interaction processes which are photocathode photoelectron emission rates to incident light flux and yield of secondary electrons from a given primary electron to the number of primary electrons. Linearity limits are attributed to the buildup of space charge effects between the last dynode stages caused by excessive anode currents [1,15]. Space charge effects that occur between the dynode interstages near the anode are compensated for with an unbalanced dynode-voltage distribution. Increasing the interstage voltages near the anode is intended to make up for excessive secondary electron emission rates from the end dynodes. Excessive cathode voltages, poor dynode interstage voltage distribution, and high incident light intensities are sources of excessive anode currents [1,15]. Operation above

the saturation anode current limit can cause fatigue effects which generate signal nonlinearities and reduce the lifetime of the PMT. Photomultiplier nonlinearity may also be attributed to hysteresis instability [1]. Hysteresis instabilities are temporary anode current instabilities that develop when a PMT is exposed to a light source.

Photomultiplier tube models EMI 9817Q and EMI 9214Q were selected based on their spectral response, gain, dark current, linearity, and speed of response characteristics that have been addressed above. Both models have fused-silica end windows for high transmission at 300 nm. They both rely on twelve linear focused dynode structures that offer high gain, good linearity, and fast time response [1,15]. EMI 9817Q has a trialkali (S20) photocathode which has a spectral response from the ultraviolet to near infrared. However, it suffers from relatively high dark currents. The bialkali photocathode used for the EMI 9214Q tube offers better ultraviolet response and lower thermionic emissions. EMI 9817Q and EMI 9214Q use BeCu and CsSb as dynode materials, respectively. The BeCu material offers the best linearity and high temperature operation [1,15]. However, this material is thought to introduce gain instabilities that will be discussed further in Section 3.1.1. The CsSb dynode material offers high gain, better gain stability, and minimum hysteresis. CsSb, as a dynode material, requires lower operating voltages, settles quicker

between changes of light levels, and has lower surface resistivity [1,15]. The most fundamental selection concern is high quantum efficiency for ultraviolet light. This criteria is important for signal-to-noise, detection, and resolution measurement properties. Both EMI 9214Q and EMI 9817Q PMT models offer relatively high quantum efficiencies at 300 nm with the EMI 9214Q consistently having higher quantum efficiency values. The EMI PMTs used in experimental procedures had quantum efficiencies that range from 22.8 to 31.5 percent. No other manufactures of PMTs were found that had as high a quantum efficiency at 300 nm.

2.2 Photon Counting Theory

The detection of weak photon fluxes is best accomplished through the implementation of a photon counting system. Photon flux is proportional to the power of the light source. Thus, a photon counting system measures a light signal by taking advantage of the discrete (photon) nature of light. The advantages presented by photon counting are that the counting procedure assigns equal weights to all detected pulses which allows for digital data processing and it also provides discrimination against pulses (noise) that have a low probability of being generated by the incident photon flux. This improves the system's operating characteristics substantially [17].

A photon counting system consists of a PMT detector, amplifier, discriminator, and digital counter as is

illustrated in Figure 2.4 [17]. The system's detector must be capable of responding to individual photons from the incident photon flux. Photomultiplier tubes are employed as the detector of choice [18]. Photon counting is a mode of PMT operation that separately time resolves photon events at the anode of the photomultiplier. PMTs offer narrow pulse width outputs and distinct single electron response spectrum characteristics [15]. Single electron response (SER) describes a detector's ability to develop an avalanche charge distribution initiated by a single electron released by photon-photocathode interaction [18]. The narrow pulse distributions (sensed in nanosecond intervals) are well suited for pulse counting schemes. The pulse shape profiles produced by the photomultiplier vary due to secondary backscattered electrons as described in Section 2.1. It is therefore necessary to choose PMTs designed to minimize the occurrence of these unwanted emissions. As the intensity of light is varied to the photon counting detector, the SER characteristic of the detector should result in area changes under the SER peak and not changes in SER peak position. The arrival of photons onto the detector interface may be regarded as independent occurrences of sequential random events at a rate equal to the incident photon flux. A Poisson distribution can be derived to describe the probability of detecting these random events. The probability $P(N)$ of N photoelectrons, resulting from low

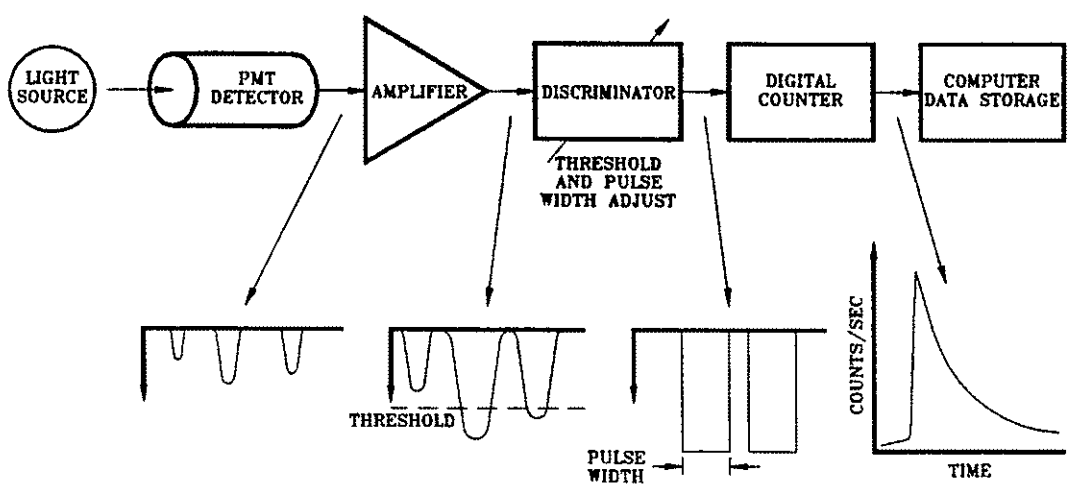

Figure 2.4. Schematic representation of a basic photon counting system.

photon fluxes incident upon the PMT's photocathode, being detected within a time period of Δt is described by the Poisson distribution:

$$P(N) = \frac{N'^{N}(e^{-N'})}{N!}, \qquad (1)$$

where N' is the average number of photoelectrons detected within Δt [2]. Understanding of the Poisson distribution of the random photon events is important for the detection of weak lidar returns used in photon counting.

The amplifier and discriminator provide the required pulse selection criteria which result in the production of a digital pulse to be processed by the digital counter [17]. The amplifier's purpose is to bring the pulsed output of the PMT to a level that is compatible with that of the discriminator. To preserve the pulse height characteristics of the PMT, the amplifier must be properly load matched with the PMT (50 ohms), preserve fast pulse rise times, have low noise input, and maintain high gain stability [1,17]. A pulse height discriminator produces digital pulses of uniform (adjustable) width which correspond to an input pulse. Pulse-pair resolution describes a discriminator's ability to recover from a previous input pulse event and be able to respond to future input pulses. A discriminator should have the shortest possible pulse-pair resolution (the 300 MHz discriminator utilized offered 3.3 nsec pulse-pair

resolution at the minimum output width setting) to ensure that received pulsed input is processed correctly and may be accounted for in data processing. Pulse pile-up occurs at high photon counting rates. Two photons could appear at nearly the same time and thus be counted as one photon and not two. Pulse overlap is expected due to the random nature of the photon events. Pulse pile-up error, ε_{PMT}, can be calculated by using the following equation:

$$\varepsilon_{PMT} = 1 - \exp^{(-\eta R t_R)}, \qquad (2)$$

where η is the quantum efficiency of the selected PMT, R is the average incident photon rate, and t_R is the discriminator width. Using a quantum efficiency of 23% (EMI 9817QA #3236), a discriminator pulse width setting of 5 nsec, and an average photon rate of 50 MHz results in a pulse pile-up error of 5.58% [19]. Therefore, pulse pile-up effects can be ignored (R < 50 MHz) by maintaining a uniform pulse shape and minimum discriminator pulse width output of 5 nsec.

Other important features to consider are the pulse height discriminator's abilities to preset a voltage threshold and an output pulse width. The voltage threshold setting allows for signals below this threshold to be ignored, thereby improving the overall system sensitivity to a selected signal of interest. Noise sources such as

Johnson (or Nyquist) noise and dark current may be eliminated with appropriate voltage threshold settings. Dark current (the result of thermionic emission) and associated noise components limit the lower level of PMT light signal detection [1]. It is important to experimentally verify the operating threshold settings. Low count rates at high discriminator thresholds will cause the counting system to miss a large fraction of the PMT signal pulses and will reduce the system's sensitivity. However, it is interesting to point out that high discriminator thresholds will reduce overall sensitivity but, at the same time, increase the maximum average observed count rates. Non-thermal noise events such as high energy particles (cosmic rays, local radioactivity decay in glass) and residual gas molecules in the detector that produce ion events may be removed through the implementation of a dual voltage discrimination device [16]. Low and high voltage threshold settings produce a signal window for analysis but may result in a reduction of system signal resolution. As the input signal pulse rates increase, pulse overlapping is inevitable. To minimize this effect, discriminator output pulse widths may be reduced. This reduction is limited only by the pulse resolution required by the circuits following the discriminator. An increase in the discriminator's output pulse width causes the observed count rates to decrease. If extremely weak light signal detection is

desired at photoelectron levels that correspond to slightly above the energy levels that cause dark current, the system's signal-to-noise ratio (SNR) will be significantly reduced. To counteract the loss in SNR, the statistics of light measurement can be improved by increasing count times. Discrete pulse counting of the pulse height discriminator output may be accomplished by many counting configurations such as direct counting, synchronous detection, or background subtraction [17]. The presented photon counting system utilizes a multichannel analyzer (MCA). A MCA counts the pulsed output of the discriminator during a specified dwell period. The MCA adds the current counts to the sum of previous counts corresponding to dwell periods of previous scans. The MCA data is linked to a computer system for analysis and storage of data.

In general, if the limits of the PMT are not exceeded, nonlinearities that arise in the photon counting system's response are due to pulse overlapping and the finite electronic response times. A photon counting system may be classified as either paralyzable or nonparalyzable system. The photon counting system used for experimental analysis is an example of a paralyzable counting classification. A paralyzable counting system is defined when a photon event fails to be recorded when the time interval between its occurrence and the occurrence of the most recent photon event is less than an extended dead time interval [20]. As

the frequency of photon events increases, a paralyzable counting system will go to zero because it is measured from the occurrence of the last event. A nonparalyzable counting system is defined when a photon event will not be recorded when the time interval between its occurrence and the occurrence of the last recorded event is smaller that the nonextended dead time [20]. The nonparalyzable photon counting system will asymptotically increase toward a maximum average count rate equal to the inverse of the nonextended dead time. A photon counting system contains components of both types of dead times. However, one dead time type will dominate and characterize the photon counting system. If two pulses, above the discriminator setting, arrive within the limits of the pulse-pair resolution of the discriminator, they will be treated as one pulse and will result in an apparent reduction of the observed or true count rate. Two pulses, having respective voltage levels below the discriminator threshold and within the limits of discriminator pulse-pair resolution, may be summed together and result in a single false count output, thus, increase the observed count rate. It is important, therefore, to take careful consideration of the discriminator threshold in order to maximize the detector's linear operation range and not to simply base the threshold selection upon maximizing the photon counting system's SNR.

2.3 DIAL Equation

Measurement of ozone concentrations and distributions in the atmosphere is important for understanding its involvement in tropospheric chemistry, pollution, and climate related processes and in stratospheric chemistry, solar ultraviolet radiation screening, and thermal equilibrium [17]. The wide spatial distribution of ozone in dynamic atmospheric areas such as the troposphere and rapid ozone depletion events makes *in situ* ozone measurements from balloons and aircraft insufficient data gathering methods [17]. A method to improve ozone detection and to address the sighted atmospheric concerns is the application of the differential absorption lidar (DIAL) technique.

The airborne DIAL measurement technique relies on the use of two pulsed, high-energy, narrow-linewidth, tunable lasers to transmit laser pulses into the atmosphere. The laser pulses excite aerosols and ozone molecules in the atmosphere, which in turn emit light. Backscattered laser energy is then captured by a large 36 cm telescope on the aircraft and directed by dichroic optics onto assigned detectors [3,4]. The backscattered light detected by the lidar system is directly proportional to the molecular density. Thoughtful selection of laser wavelengths provides the sensitivity required to accurately measure the ozone concentrations present in the atmospheric region under investigation. One laser is tuned to the ozone absorption

line (on-line), and the other laser is tuned to a nearby spectral region that has little or no absorption by ozone (off-line). Recent tropospheric lidar sensing used on- and off-line wavelengths of 289 nm and 300 nm, respectively, transmitted in the nadir direction. Stratospheric investigations in the zenith direction utilized wavelengths of 301 nm for on-line and 311 nm for off-line [18]. The on- and off-line lasers are controlled to produce sequential laser pulse pairs with a time separation of 300 μsec at a repetition rate of 30 Hz. The sequential laser pulse train is necessary to ensure that the same atmospheric scattering volume is sampled by both wavelengths during the DIAL measurement [18,20].

In order to measure the density of ozone in the atmosphere as a function of range, the backscattered laser power must be measured. The backscattered power $P(R)$ at the operating laser wavelength, applicable to the 300 nm region, from range R is given by:

$$P(R)\,R^2 = \gamma\,B(R)\exp\{-2\int_0^R [\beta(R) + n(R)\,\sigma]\,dR\}, \qquad (3)$$

where γ is the lidar system constant at the operating wavelength, $B(R)$ is the total atmospheric volume backscatter coefficient, $\beta(R)$ is the total atmospheric optical extinction coefficient neglecting absorption by ozone, $n(R)$ is the ozone number density, and σ is the ozone absorption

cross section [21]. A general solution can be found for the ozone number density profiles as a function of the on- and off-line lidar wavelengths:

$$n(R) = \frac{1}{2(R_2-R_1)(\sigma_{on}-\sigma_{off})} \ln \frac{P_{off}(R_2)\,P_{on}(R_1)}{P_{off}(R_1)\,P_{on}(R_2)} \quad [M]$$

$$-\frac{1}{2(R_2-R_1)(\sigma_{on}-\sigma_{off})} \ln \frac{B_{off}(R_2)\,B_{on}(R_1)}{B_{off}(R_1)\,B_{on}(R_2)} \quad [B]$$

$$-\frac{1}{(\sigma_{on}-\sigma_{off})}(\beta_{on}-\beta_{off}), \quad [E] \qquad (4)$$

where R_2-R_1 is the range interval over which the average ozone concentration is calculated, σ_{on}-σ_{off} is the difference between the ozone absorption cross-sections of the on- and off-line lasers wavelengths, P_{on} is the power received from the on-line laser at either R_1 or R_2, and P_{off} is the power received from the off-line laser at either R_1 or R_2. If the on- and off-line lasers are sampling the same atmospheric volume, then backscattered error term, *[B]*, approaches zero and can be neglected. Likewise, the extinction error coefficient, *[E]*, will be negligible if the on- and off-line laser wavelengths are kept relatively close. Further error analysis can be found in references [3,17,21-25]. The end result from the approximations is the general DIAL equation

used to determine $n(R)$:

$$n(R) = \frac{1}{2(R_2-R_1)(\sigma_{on}-\sigma_{off})} \ln \frac{P_{off}(R_2)P_{on}(R_1)}{P_{off}(R_1)P_{on}(R_2)} . \quad (5)$$

It should be noted that the actual ozone measurement is based on a ratio of PMT output voltages and not power. A volume mixing ratio of the number density profile can be calculated by dividing the gas number density by the ambient atmospheric number density [3]. The DIAL measurement technique and the number density profile equation above result in the remote measurement of atmospheric ozone profiles [3,4].

DIAL measurements are subject to various random and systematic errors [3]. Errors that may be generated and that require corrective measures for photon counting experiments are uncertainties in Poisson statistics in the backscattered signal, uncertainty in the ozone absorption cross sections for the chosen DIAL wavelengths, nonlinearities in photomultiplier detection electronics, and contributions of aerosol extinction and backscattering effects [26]. Random errors are due to noise effects in the return signal. The main sources of random errors are photon statistic variabilities, detector dark currents, and background signal noise. The effects can be minimized by maximizing the system's overall signal-to-noise ratio. This

may be accomplished by maximizing the laser pulse energies, increasing laser pulse repetition rate, improving receiver optical throughput, using detectors of higher quantum efficiency and lower dark current, and selecting a narrow band optical filter that maintains high optical transmission of the on- and off-line return wavelengths while rejecting background daylight. Random errors may also be reduced, following data acquisition, by averaging the returned data in such a way to achieve a balance between measurement precision and spatial resolution. Systematic errors in DIAL measurements are caused by both atmospheric and instrumental influences. The on-line laser should have a narrow

Nd:YAG Pump Lasers(2)	
pulse separation, μsec	300
repetition rate, Hz	30
pulse length, nsec	15
transmitted laser energy at 532 nm, J	1.6
Dye Lasers (2)	
laser linewidth at 300 nm, pm	<4
transmitted laser energy at 300 nm, mJ	50

Table 2.1. Airborne DIAL transmitter characteristic values.

linewidth and a high spectral purity. The effects of signal overloading should also be avoided which introduce signal nonlinearities in the data analysis [3]. Table 2.1 lists typical ozone DIAL measurement operating system parameters [21,22]. See Appendix C for additional system description and a system schematic.

2.4 Photon Counting for Lidar Measurements of Stratospheric Ozone

Photon counting provides the most favorable measurement method of continuing ozone atmospheric detection below the limits of analog measurements. A photon counting system should be implemented when the backscattered light signal drops below count rates of 10^7 photons per second [18]. A ground based lidar facility, utilizing PMTs operated in the photon counting mode, has been designed to measure ozone concentrations in the stratosphere range of ~15-45 kilometers [26]. Data values obtained from ground based and airborne DIAL atmospheric detection systems are important for studying the dynamic properties of the atmosphere. With detailed experimental analysis of the DIAL operating parameters and detailed photon counting system evaluation of individual PMT characteristics, proper photon counting system operation can be attained.

CHAPTER III

EXPERIMENTAL SETUP

3.1 The Photon Counting System

Photon counting utilizes the unique characteristic of a photomultiplier tube's ability to detect single photon events. In this mode of detection, photon events are isolated at the anode of the photomultiplier then counted by a scaler. Employing this method will allow for extended range measurement of atmospheric species whose signals are below the level of analog detection. The photon counting experimental setup is shown in Figure 3.1 and an explanation of individual components follows.

3.1.1 Photomultiplier Tubes

Two end-window PMT models were used for performance evaluations. THORN EMI series models 9214Q and 9817Q were chosen for their high gain, high speed, dynamic range, signal linearity, and well defined single electron resolution. The Q notation is used to indicate that a fused-silica end window is incorporated as apposed to a borosilicate glass end window. Both PMT models relied on the quartz end window for extended ultraviolet light response.

The EMI 9817Q has been the preferred PMT for ozone DIAL signal processing. This 12-stage, linear-focused PMT utilizes a S20 (Na-K-Sb-Cs) photocathode with BeCu dynodes.

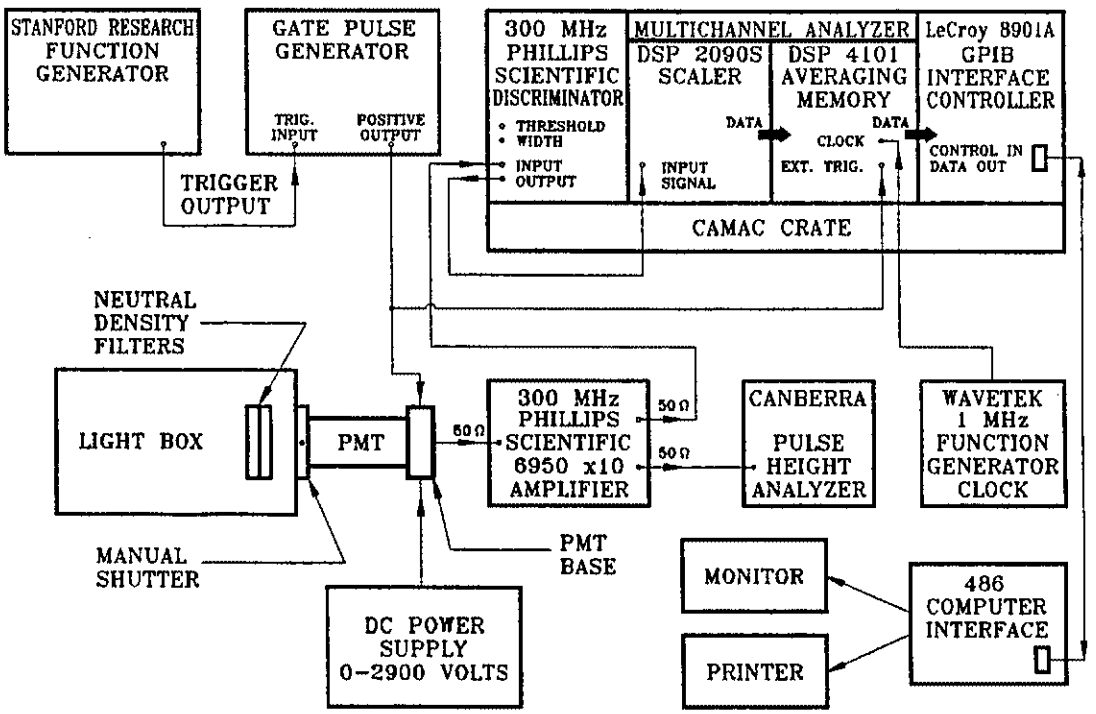

Figure 3.1. Photon counting experimental setup.

Our measurements and the work of Barrick, Lee *et al.*, and Bristow *et al.* confirmed the existence of signal gain instability [27-29]. Referred to as a "signal induced gain change", the effect is evident when a gated PMT is exposed to a constant light source or when an ungated PMT is exposed to a light pulse during the ungated period [28]. The signal gain instability is believed to be due to the effects of impurity ions released from the BeCu dynode chain surfaces.

In an attempt to reduce this effect, the EMI 9214Q was selected as a possible replacement to the EMI 9817Q. This is also a 12-stage, linear-focused PMT. However, changes have been made with respect to a bialkali (Sb-K-Cs) photocathode and CsSb dynode material. The CsSb dynode material has been found to reduce the signal gain instability [28,29].

PMT performance characterization is accomplished by exposing the PMT, mounted externally to a light-tight enclosure, to light produced by a xenon lamp [27]. The PMT and attached base are mounted on a manual shutter housing lined up in a direct optical path from the xenon light source. Neutral density filters placed directly in front of the PMT's faceplate are used to examine linear and operating characteristics of a selected PMT. Operating under various design variables, the optimum PMT operating parameters are determined and used for later inflight operations with the lidar laser system.

3.1.2 Preamplification

Preamplification of the PMT's pulsed output is necessary for discriminator analysis. The output of the PMT is typically in the low millivolt range and of several nanosecond pulse width for single photon events. Amplification of such signals requires the amplifier to have low signal attenuation, low noise, high bandwidth, and fast time response. Two amplifiers were analyzed: the Phillips Scientific Model 6950 DC-300 MHz non-inverting bipolar amplifier with a voltage gain of ten and the Stanford Research Systems Model SR445 DC-300 MHz non-inverting fast preamplifier with a voltage gain of five per channel, where up to three channels may be cascaded. Both amplifiers provided acceptable operating characteristics. Preference of either amplifier depends on the total signal amplification desired. An advantage of the SR445 preamplifier was that it allowed for microvolt calibration of its input and output connections to remove any unnecessary bias amplification. In the experiments described the Phillips Scientific preamplifier was used.

3.1.3 Discriminator

The output from the PMT and preamplifier is a sum of signal and noise pulses. To isolate the lidar signal return, it is necessary to remove the noise pulses efficiently and to minimize signal losses. A Phillips Scientific 300 MHz discriminator is used to remove the noise

pulses which also result in improving the system's signal-to-noise ratio (SNR). The noise pulses are removed by determining the optimum setting of the discriminator's threshold level that will discriminate against the noise pulses but record the photon generated pulses. This maximizes the SNR. The threshold level could be varied over a range of -10 mV to -1 Volt by a potentiometer, with the operating level determined by experimentation to be discussed in the Chapter IV. The output of the discriminator is used to drive the computer-controlled pulse counting multichannel analyzer. The pulsed output of the discriminator is based on NIM logic into 50 ohms. The discriminator output pulse width could be adjusted from 2 nsec to 50 nsec. Pulse width adjustment is necessary to minimize the occurrence of pulse pile-up error.

3.1.4 Multichannel Analyzer

A DSP Technology Inc. Model 2190 Multichannel Averager (MCA) is used to count and sum the pulsed output from the discriminator. A MCA divides the incoming signal into time segments (bins) called dwell periods. The sum of all the dwell periods, specified by a programmed record length, is equal to one scan or sweep. The total number of sweeps is controlled by programmed input. The Model 2190 functions by counting the number of incoming discriminator pulses during a specified dwell period. The counts are then added to the sum of previous counts made which correspond to dwell

periods of previous scans. The end sum is the total number of counts for each dwell period. The MCA is synchronized with the PMT gate signal by an external trigger provided by the pulse generator. A clock signal, produced by a separate function generator, controls the MCA dwell time period normally set at 1 μsec. The record length set for expected lidar returns is normally 300 μsec (300 dwell periods).

The Model 2190 is physically composed of two interconnected modules, Model 2090S and Model 4101. The Model 2090S is a high speed scaler capable of counting at up to a 100 MHz rate and a maximum count of 65,535 (16 bits). The Model 4101 is a high speed averaging memory module. The basic operation of the two models is as follows: 1) The 4101 is programmed for the number of data sweeps, the number of dwell periods per sweep (or information data bins), and its memory is reset. 2) The 2090S is then enabled for counting. 3) The 4101 receives a 30 Hz trigger signal and then enables dwell clocks to latch data in the 2090S. 4) After each dwell clock, data is transferred and added to previous data in the 4101 memory. 5) After the programmed number of dwell periods have been cycled, one sweep is completed. When the programmed number of sweeps (see above) has been completed, the 4101 stops for readout over the CAMAC controller [30].

3.1.5 Computer and CAMAC Interface

The CAMAC interface crate controller provides the means, through digital control, to send or receive commands or data from individual CAMAC modules to an external computer. A 486 computer provided the necessary control of the CAMAC modules and data output with the addition of a general purpose interface bus (GPIB) module. The GPIB controlling software used was a NI-488.2 MS-DOS standard. The user control software was a Visual C++ program modeled by the MCA basic operation procedure previously outlined. Photon counting data is stored in a computer file for information analysis. A photon counting computer program for controlling commands and data transfer has been included in Appendix A.

3.2 Photomultiplier Tube Measurement System

A PMT measurement and evaluation system was constructed and is shown in Figure 3.2. Such a system is necessary for accurate and controlled PMT evaluation. Testing under known conditions ensures proper PMT response during field ozone airborne measurements and minimizes operating uncertainties. The system components will now be discussed in detail.

3.2.1 Xenon Lamp Light Source

PMT evaluation requires a wide dynamic range of light of variable intensity and wavelength. The light source used for PMT evaluation is shown in Figure 3.2. A 1000 W xenon lamp is housed inside a forced air cooled lamp housing. The

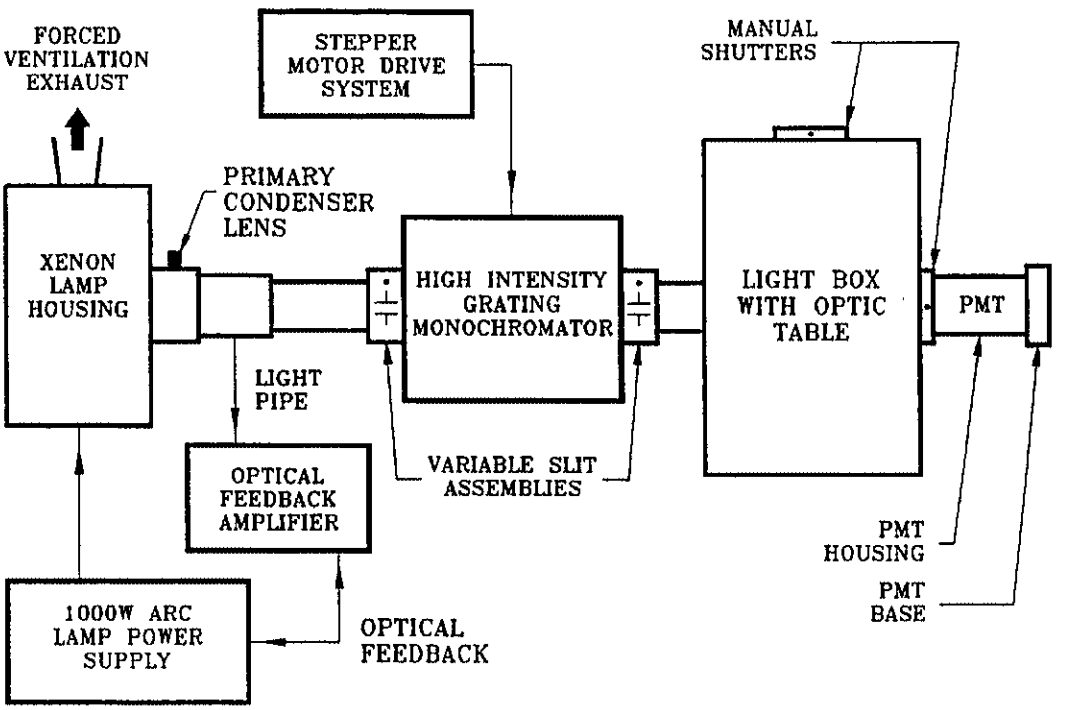

Figure 3.2. Light source schematic utilized for photomultiplier tube evaluation.

forced ventilation provided cooling for the high pressure lamp as well as removal of ozone produced from operation of the xenon lamp. The lamp housing also provided an adjustable rear reflector coated for maximum ultraviolet reflectivity. A 57 mm condenser lens consisting of two plano-convex elements was placed in the lamp housing's optical axis for beam focusing adjustments [31].

Power to the xenon lamp was provided by an arc lamp DC power supply. The xenon lamp's power supply was adjusted to 25 amperes DC and 20 volts DC once the arc lamp power supply had reached operating conditions. The arc lamp DC power supply was also coupled with an optical feedback amplifier aligned with the lamp housing's optical axis. The optical feedback amplifier function is to stabilize the xenon lamp's output against noise due to arc wander, mechanical vibration, and voltage line ripple. The optical amplifier provides stability under 0.1% ripple to the xenon lamp [31].

Light from the xenon lamp is directed into a high intensity grating monochromator. The grating used provided a wavelength range of 180 to 800 nm displayed on a three digit counter in increments of 0.2 nm. Entrance and exit variable slit assemblies attached to the monochromator provided for slitwidth control between 0.01 to 6.00 mm displayed in 0.01 mm increments. An integrated stepper motor drive system provided for precise wavelength location [31].

3.2.2 Detector Box

PMT testing is accomplished by exposing a PMT to light under controlled conditions. Evaluation is performed using a light-tight box which supports two manual shuttered housings on which a PMT housing may be mounted. One manual shutter is aligned directly with the optical path of the xenon lamp. The other manual shutter is offset at an angle of 90° from the optical axis. The inside walls of the light-tight box are of anodized aluminum which are used to isolate a horizontal optic table. The optic table is used to accommodate various optic mounts and devices (neutral density filters, beam choppers, *etc.*).

3.2.3 Pulse Height Analyzer

A pulse height analyzer (PHA) was integrated into the photon counting system in order to investigate the pulse height distribution of individual PMT's. A Canberra Series 10 Portable Multichannel Analyzer was used to read the PMT's pulse height distribution which was recorded and printed out. A simplified pulse height distribution is shown in Figure 3.3 [1]. The figure illustrates three distinct regions in the pulse height distribution. Region A is the result of inherent circuit noise, secondary emission from dynodes, and some single electron events. The distribution of Region B is due to single photon to single electron conversion which occurred at the photocathode. Region C defines PMT response to cosmic radiation, radioactive

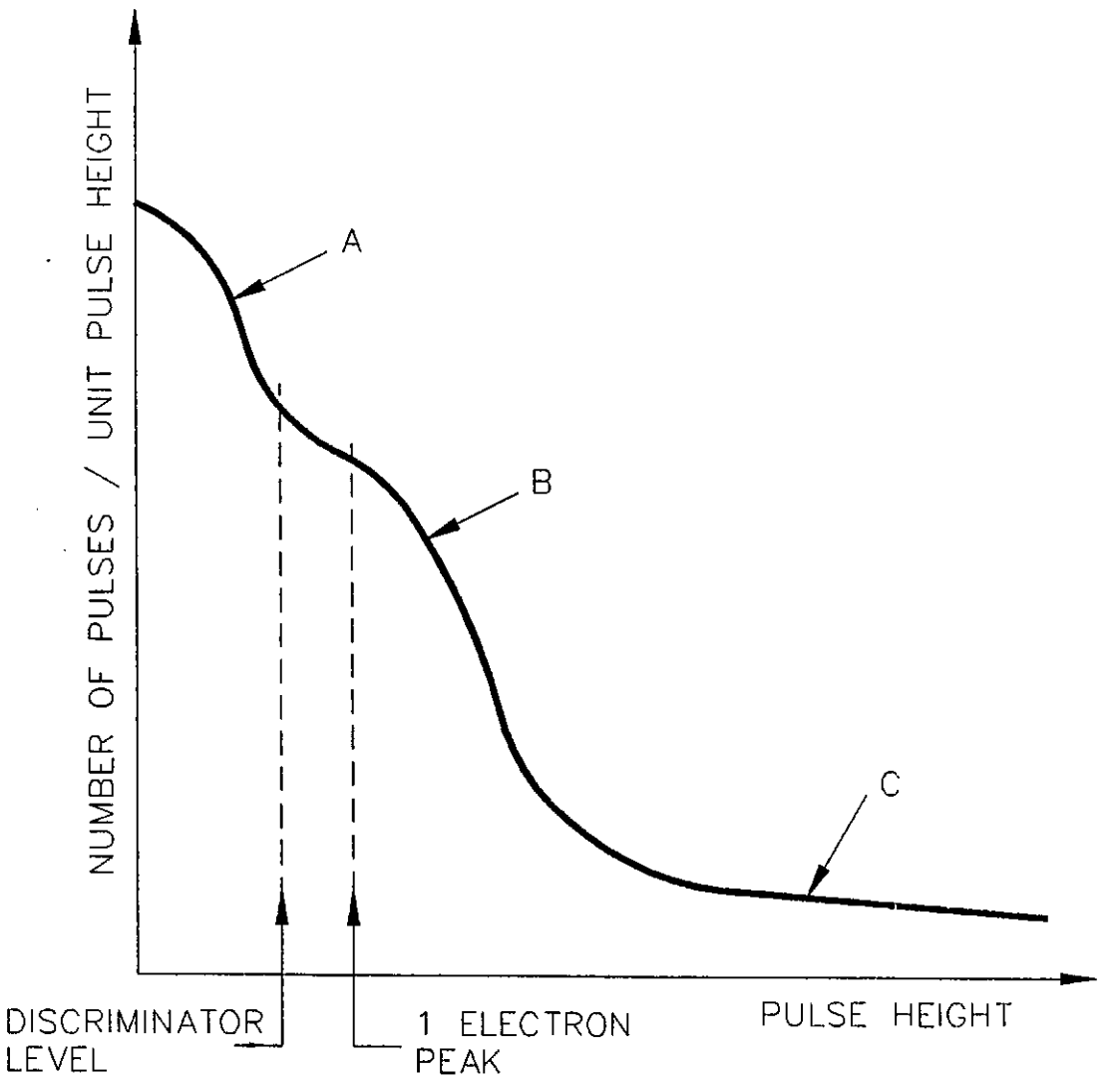

Figure 3.3. A simplified pulse height distribution for desired discriminator pulse height setting.

contaminants in tube materials, and effects of after pulsing [1]. This analysis provided the required discriminator threshold settings by determining which pulse height values isolated the single electron response region from the inherent circuit noise.

3.3 Photomultiplier Tube Base

Photomultiplier tube base voltage divider networks may be exclusively resistive or coupled with series connected capacitors. The divider networks are necessary to distribute voltage from the high voltage DC power supply to individual dynodes of the dynode chain [1]. The particular voltage divider network design depends upon the desired PMT application. The voltage divider design chosen for most of the experimental operation was the previously designed and tested focused grid gated, capacitor coupled network. This voltage divider schematic is shown in Figure 3.4. The design is intended to take advantage of the pulsed nature of the incident lidar return signals. It was found through experimental and field measurements that this particular voltage divider design and gating scheme were subject to excessive ultraviolet light bleedthrough. An attempt to remedy this problem resulted in the construction of a second voltage divider base for evaluation [28]. The result was a four dynode gated, capacitor coupled network that is shown in Figure 3.5.

Both network designs use anode grounding which allowed

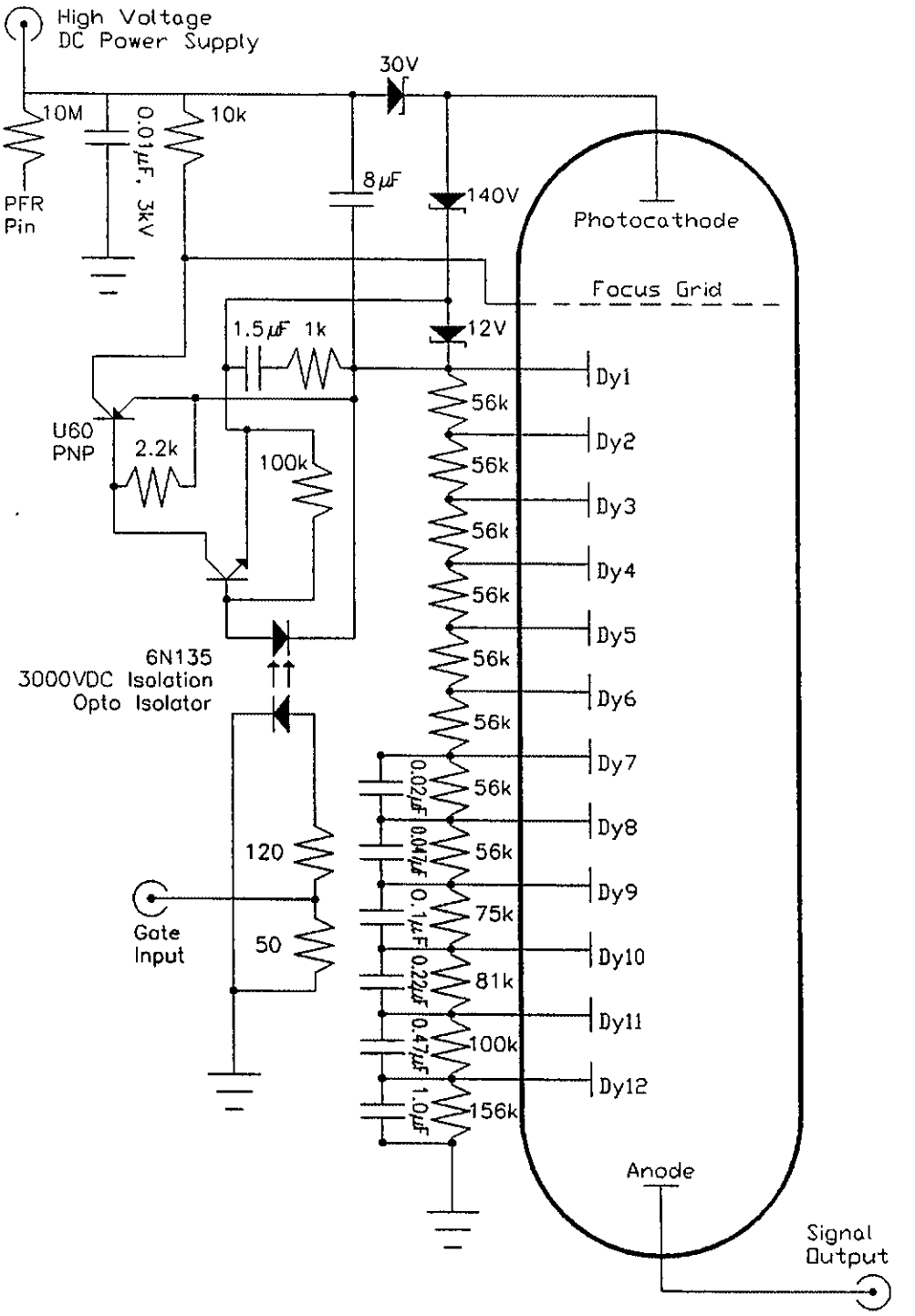

Figure 3.4. Focused grid gated, capacitor coupled voltage divider network.

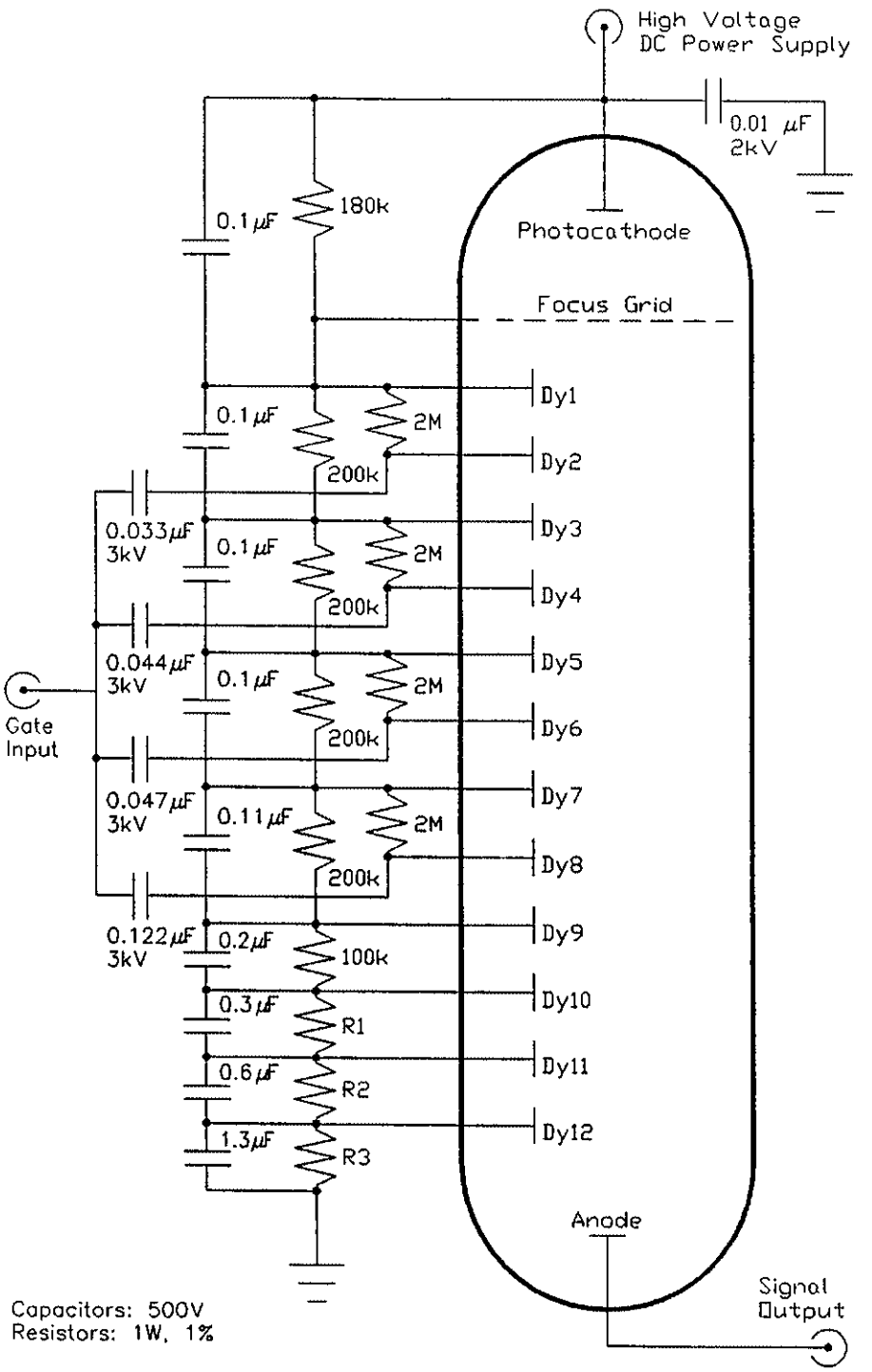

Figure 3.5. Four dynode gated, capacitor coupled voltage divider network.

for direct coupling of the PMT anode output to an amplifier or oscilloscope which was properly loaded at 50 ohms. A gate signal, produced by an externally triggered pulse generator, is used to turn a PMT "on" and offers protection to the PMT and the attached base circuit network. The gate signal protects the PMT from the exposure to intense laser near-field backscatter, including the effect of high current induced damage to the last few dynodes next to the anode. Gating prevents the premature discharging of the series coupled capacitors which help maintain the voltage at the end of the dynode chain. Gating also prevents PMT saturation and capacitor discharge due to long term exposure to solar background during daytime operations [1,27].

3.3.1 Focus Grid Gating

Gating of a PMT's focus grid presents the simplest approach to providing protection to the PMT from the harmful effects of nearfield backscattered laser light. The gate signal applied in Figure 3.4 is a TTL signal provided by a pulse generator. The gate frequency is governed by the DIAL laser operating system (current laser operating frequency is 30 Hz).

The voltage divider network distributes the negative polarity voltage from the high voltage DC power supply along the twelve dynode interstages. The tapered capacitors installed in parallel with the last six resistors in the divider chain are selected to store sufficient charge to

maintain voltage (gain) stability for the duration of a pulsed event. The signal from the PMT is monitored from the anode terminated into a 50 ohm load [1,15].

The PMT is considered "gated-off" with no gate signal applied and a high voltage DC negative polarity maintain on the base network. In this state, the potential across the 10 kΩ resistor is zero and the focus grid is at a 30 volt higher potential than that of the photocathode due to the 30 volt drop across the Zener diode. Thus, any electron released from a photon incident upon the photocathode will not be accelerated across the more negative focus grid potential and will therefore not be accelerated through the dynode chain to reach the anode.

The PMT is considered "gated-on" when a positive TTL gate signal is applied. The gate signal is transmitted across the opto-isolator boundary and acts to properly bias the PNP transistor. With the PNP transistor conducting, a potential difference is developed across the 10 kΩ resistor and the focus grid potential becomes positive with respect to the photocathode. Now, when a photon acts to free an electron from the photocathode, the electron will be accelerated across the positive potential across the focus grid and continue the amplification process through the dynode chain until it reaches the anode.

3.3.2 Four Dynode Gating

Four dynode gating of a PMT provides greater protection

from backscattered laser returns, but adds additional complexity to the gate circuit design. The gate signal applied to dynodes 2, 4, 6, and 8 shown in Figure 3.5 is provided by an externally pulsed gate board that is shown in Figure 3.6. The pulsed gate board receives a TTL signal corresponding to the controlling frequency of the DIAL laser system and sends out a high voltage pulsed signal to gate the PMT that is regulated by the 0-200 volt DC power supply. Gating of dynode 1 is avoided since a higher than normal gain is necessary to ensure proper coupling with the rest of the dynode chain. Applying a gate signal to the remaining dynodes is not recommended due to the significant signal generation from their surfaces [28].

A voltage divider network is used to distribute the ~3000 volt negative polarity voltage along the twelve dynode interstages. The 0.1 μF capacitors across the first five stages were necessary to ensure gate turn on within 0.1% of full amplitude in less than 1 μsec. The tapered capacitors across the last four stages in the divider chain are selected to maintain voltage (gain) stability for the duration of a pulsed event. Resistors R1, R2, and R3 of the last three dynode stages were necessary for attaining good signal linearity. Values of these three resistors need to be optimized for every particular PMT operated. Termination into a 50 ohm load allowed for proper signal analysis of the anode's output [28]. An additional complication of this

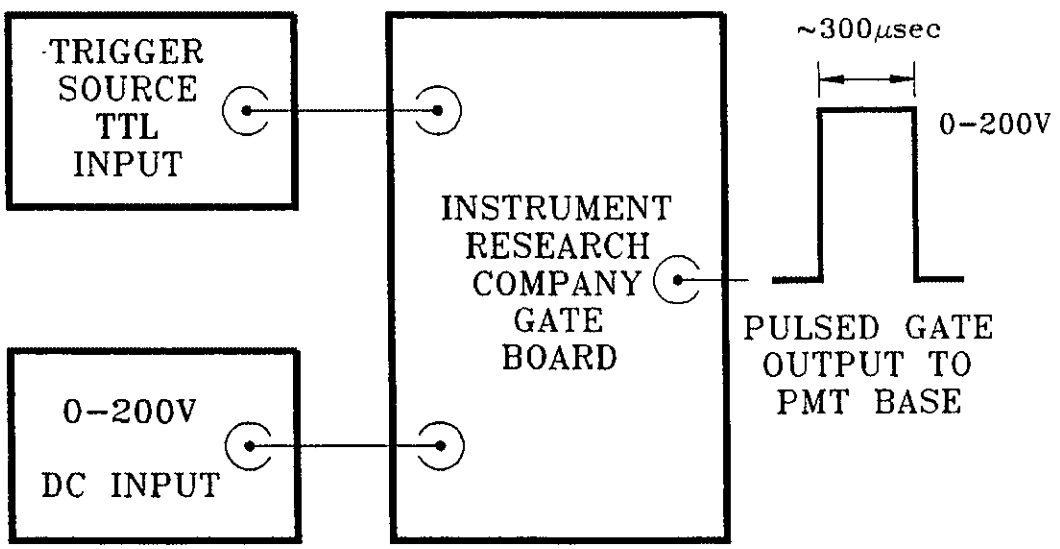

Figure 3.6. A simplified schematic of the externally pulsed gate board utilized if four dynode gating techniques.

scheme is that the 0-200 volt DC power supply must be optimized for a given PMT supply voltage.

With no gate pulse present and a high DC voltage of negative polarity applied to the cathode, the PMT is considered "gated-off". In this condition, the potentials across each 2 MΩ resistor are zero. Therefore, the potential difference across dynodes 1 and 2, dynodes 3 and 4, dynodes 5 and 6, and dynodes 7 and 8 are zero as well. Now, any electron released from the photocathode by an incident photon would be accelerated across the focus grid but would not be able to continue through the dynode chain due to the lack of further positive potential differences.

The PMT is considered "gated-on" when a positive gate pulse is applied. The gate signal creates a potential difference across each 2 MΩ resistor that results in a positive dynode voltage differential with respect to the previous gated dynode. When a photon incident onto the photocathode frees an electron, the electron will be accelerated and amplified across the positive potentials of the focus grid and dynodes until it reaches the anode.

CHAPTER IV

EXPERIMENTAL RESULTS

This Chapter will discuss the experimental results obtained from the setup presented in Chapter III. Selected PMTs were evaluated to establish noise and saturation count rates, cathode voltage operating ranges that yielded constant signal-to-noise ratio, and linearity performance characteristics. Photon counting experiments were then conducted to identify setpoints for the discriminator's voltage threshold and pulse width that would maximize each PMT's linear operating region. Once these measurements were completed, holdoff characteristics of the focus grid and four dynode gating designs were conducted and discussed. Final measurements taken were that of actual photon counting results utilizing the lidar ozone detection system and comparing these results to those attained by the analog measurement method.

4.1 Photomultiplier Tube Characteristics

Photomultiplier tubes of the same series, manufactured under similar conditions by the same manufacture, will still each have different operating characteristics. Therefore, individual analysis of photomultiplier tubes is required for the proper determination of their operating characteristics required for implementation in a photon counting system. After an exhausted review of related literature,

photomultiplier tube models EMI 9817Q and EMI 9214Q were selected for photon counting measurements due to their high quantum efficiency in the ultraviolet wavelength spectrum and easy incorporation into the DIAL atmospheric detection system. The tests presented here were conducted to develop an understanding of individual PMT responses and to determine the optimum operating tube characteristics. Uniform PMT current gains were selected to allow for PMT comparisons from the gathered experimental test results. Tube gain was set by the respective PMT cathode voltage that corresponded to a current gain of 1.5×10^7 as read from the PMT's gain versus cathode voltage curve (see Figure 2.2). Evaluation of PMT current gains and quantum efficiencies were performed by Burle Industries. Photomultiplier test results have been summarized and are listed in Table 4.1.

4.1.1 Noise Count Rates

Measurements of PMT noise counts in the photon counting system were performed to identify the amount of noise introduced into the counting system by operation of the PMT detector. The insertion of a PMT from its protective storage container into the PMT base socket and magnetic shielding resulted in short term exposure to ambient light. It is recommend that a PMT be allowed to reach an equilibrium condition over a 24 hour settling period [1,15]. Noise measurements were taken from the time a PMT was

MANUFACTURE SERIAL#	PHOTO-CATHODE MATERIAL	DYNODE CHAIN MATERIAL	QE @ 300 nm (%)	VOLTAGE FOR GAIN OF 1.5×10^7 (Volts DC)	NOISE @ 70 mV DISCRIMINATOR THRESHOLD (counts/sec)	CONSTANT SNR OPERATING RANGE	SLOPE OF OUTPUT SIGNAL (mV/microsec)	SIGNAL CHANGE DURING GATE ON @ 2 VOLTS OUT (mV)	OPTIMIZED DISCRIMINATOR THRESHOLD @ 30 Hz (mV)
EMI 9214QA #5156	BIALKALI Sb-K-Cs	CsSb	26.6	1525	16100	1200-1600	0.22	100	110
EMI 9214QB #5150	BIALKALI Sb-K-Cs	CsSb	31.5	1300	21950	1175-1475	-0.28	-130	110
EMI 9214QB #5162	BIALKALI Sb-K-Cs	CsSb	25.2	1280	16000	1200-1575	0.07	30	100
EMI 9817QA #3167	S20 Na-K-Sb-Cs	BeCu	25.2	2670	87500	2300-2700	-0.54	-250	140
EMI 9817QA #3233	S20 Na-K-Sb-Cs	BeCu	28.3	2400	209000	2175-2450	-0.17	-80	150
EMI 9817QA #3236	S20 Na-K-Sb-Cs	BeCu	23.2	2260	296100	2050-2400	-0.11	-45	105
EMI 9817QA #3283	S20 Na-K-Sb-Cs	BeCu	23.6	2070	381600	1950-2300	-0.37	-170	110
EMI 9817QA #3285	S20 Na-K-Sb-Cs	BeCu	22.8	2375	254500	2175-2450	-0.33	-150	105

Table 4.1. Photomultiplier tubes used for photon counting.

inserted into the tube base, in specific time intervals, to study the noise effects.

The output of the PMT under investigation was connected to the photon counting system. A discriminator threshold of 70 millivolts was selected to eliminate variations in the noise data due to spurious noise pulses. The discriminator pulse width was set at five nanoseconds. The multichannel analyzer (MCA) was programmed for 50 sweeps and 400 record length, relying on a one megahertz clock signal and external trigger of 30 hertz. The total photon counting time interval was 1.67 seconds. Ten noise count measurements were taken and averaged for the final noise count value. This final noise count value was then converted to counts per second and listed as shown in Table 4.1. For optimum photon counting experimental results, PMTs with the lowest noise count rates should be selected. As seen in Table 4.1, the EMI 9214Q series provides the lowest overall noise count values when compared against the EMI 9817Q series.

4.1.2 Discrimination Threshold and Pulse Width

Once the operating characteristics of the PMT had been identified, setpoints for discriminator operation must be determined. The signal from the PMT is amplified and then sent to the discriminator. The only adjustment on the amplifier was to ensure that the amplifier's bias setting was adjusted to zero prior to any photon counting measurements. However, for proper discriminator operation,

discriminator voltage threshold and pulse width was to be verified for each PMT utilized in the experimental setup. The discriminator setpoints were important in regards to the photon counting system's classification as a paralyzable or nonparalyzable system (as defined in Section 2.2) and to ensure maximization of the linear operation capabilities of the counting system.

Minimizing the discriminator pulse width is important in order to minimize the effects of pulse pile-up and to ensure that each photon event is accounted for in data analysis. Pulse width analysis was carried out in the photon counting experimental setup as shown in Figure 3.1. The PMT to be analyzed was allowed to reach the 24 hour equilibrium condition prior to discriminator analysis. Once this condition had been reached, the discriminator voltage threshold was set at its minimum setting (10.5 mV) and pulse width was set to five nanoseconds, to be adjusted in five nanosecond intervals between 5 and 40 nsec. A neutral density filter was utilized in the linearity measurements that resulted in a normalized ratio of pulse counts without the neutral density filter (N) to pulse counts with the neutral density filter (Nf). The ideal linear ratio of N/Nf times the transmittance of the neutral density filter yields a value of 1.5. Increases in PMT count rates were set by incremental slit widths adjustments of the 300 nanometer light produced by the xenon lamp. In Figure 4.1, evidence

of pulse pile-up is demonstrated by a continued decrease of pulse counts as the discriminator pulse width is increased. It is also apparent from this figure that the photon counting system is a paralyzable classification and has the longest linear operating range at the shortest discriminator pulse width. The wide variability (below 100 kHz) of the normalized pulse count ratio is attributed to the random pulsed nature of the photon events. Measurement of pulse counts should always consider minimizing errors associated with pulse pile-up. Calculation of the pulse pile-up error (Equation (2), Section 2.2, EMI 9214QB #5162) yielded results that agreed with the measured results as shown in Figure 4.2. From repeated pulse counting measurements, the discriminator pulse width to be used for continued photon counting measurements was determined to be five nanoseconds. This pulse width value ensured the highest possible count rate (50 MHz), longest linear operating region, and lowest pulse pile-up errors (<5%) and it was also compatible with the signal input requirements of the MCA.

Evaluation of discriminator voltage threshold settings were performed to verify discriminator analysis results noted by Donovan *et al.* [20] with respect to either paralyzable or nonparalyzable counting system response and to ensure linear photon counting system response. Voltage threshold analysis was performed under the same conditions as the pulse width analysis with the following exceptions:

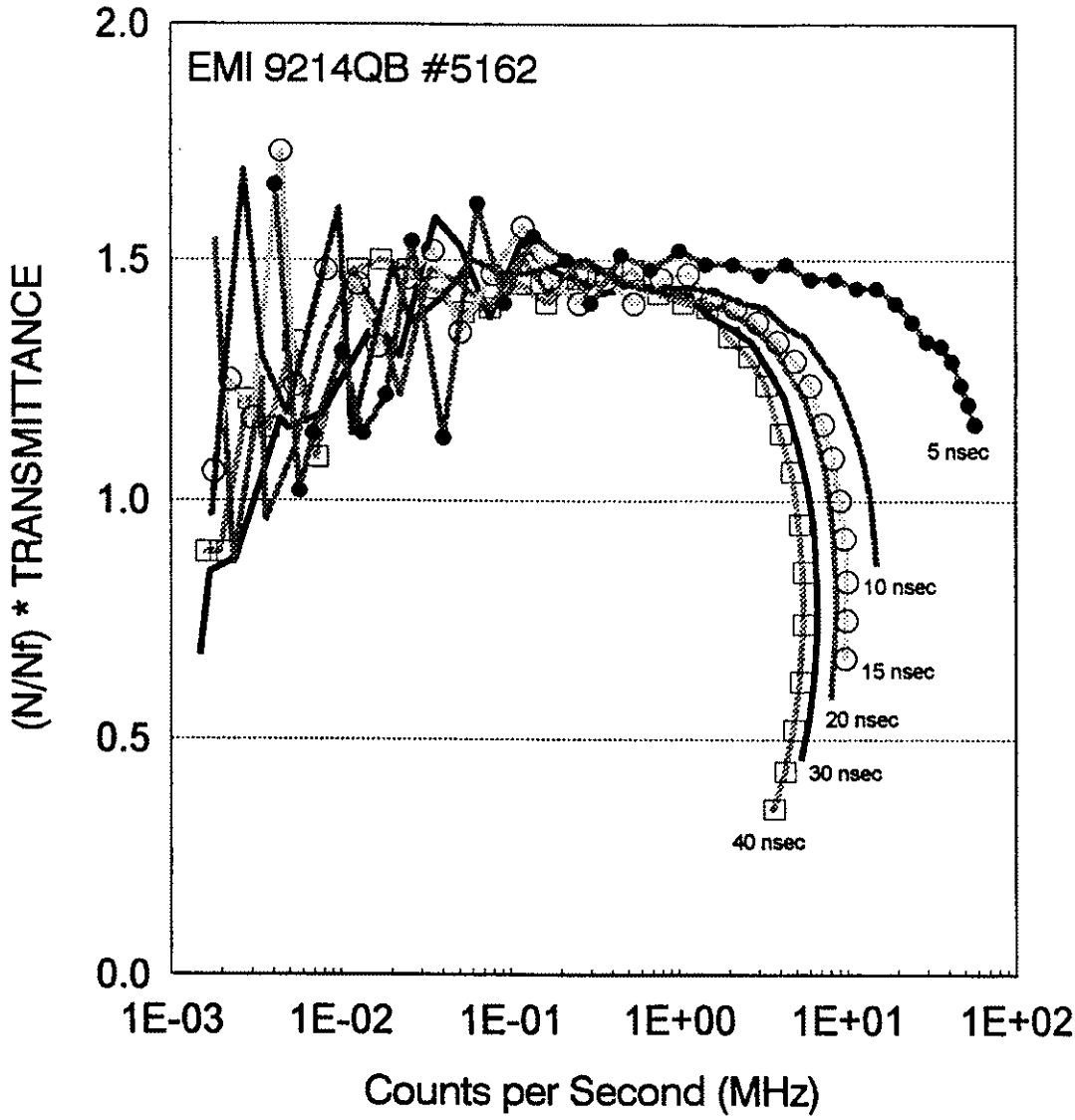

Figure 4.1. Photomultiplier pulse pile-up measurements indicating the nonlinear effects introduced by increasing discriminator pulse widths.

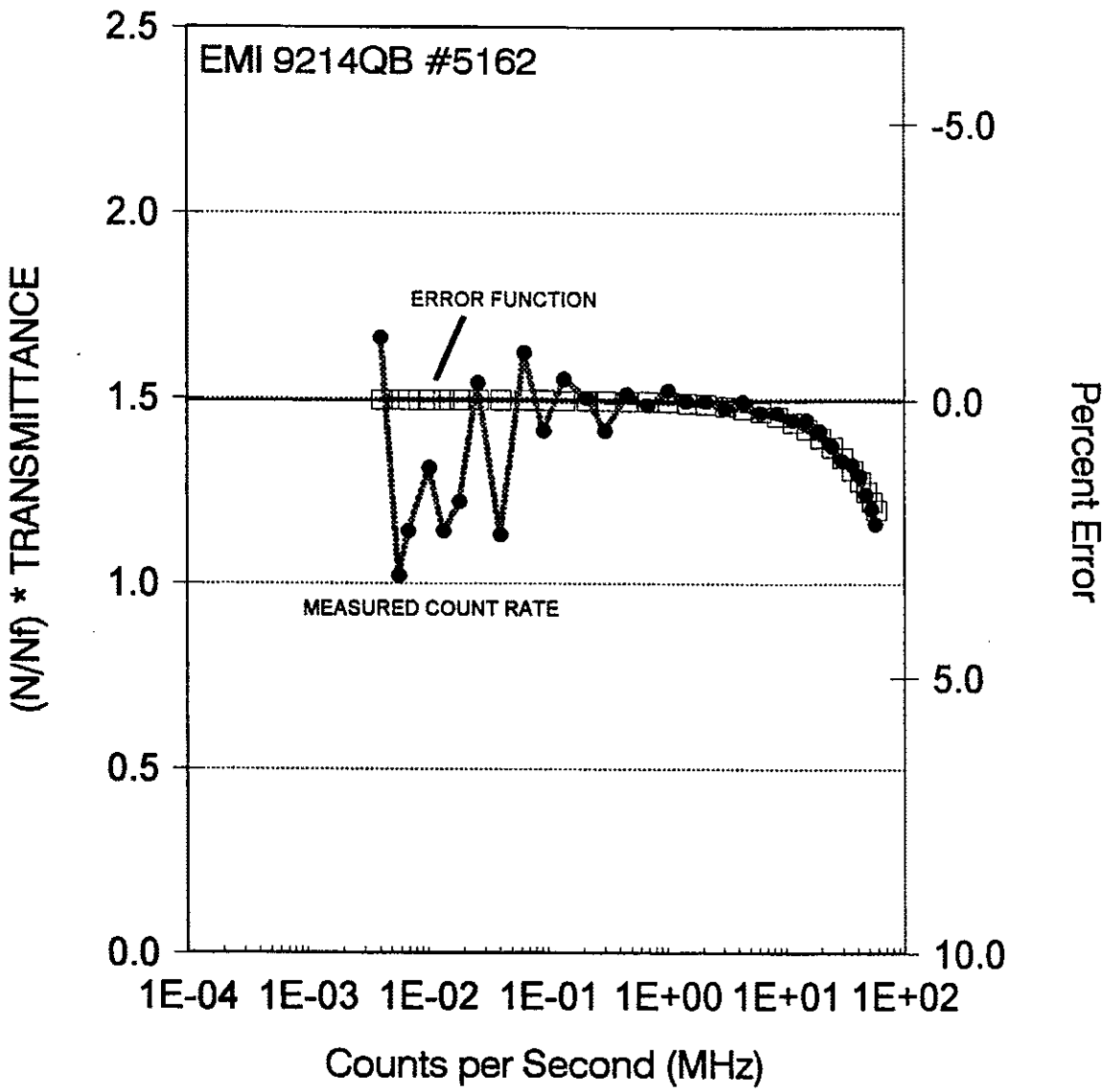

Figure 4.2. Pulse pile-up error function correlation with actual photon counting measurement.

discriminator pulse width adjusted for a five nanosecond pulsed output and discriminator threshold adjusted in increments of 10 millivolts between successive measurements. Improper threshold settings result in photon events that are not detected which lead to signal nonlinearities and can alter the overall photon counting system signal output classification as either paralyzable or nonparalyzable (see Section 2.2). The measured photon counting threshold response results duplicated the results attained by Donovan *et al.* [20] as shown in Figure 4.3. Deviation from the optimum voltage threshold (110 mV) for EMI 9817QA #3283 produced unsatisfactory results. That is, significantly high voltage thresholds (200 and 250 mV) caused the photon counting system count rate to increase exponentially from the proper linear response as described by a nonparalyzable system. Likewise, voltage thresholds (80 mV) below the optimum threshold resulted in photon counting rates that represented those of a highly paralyzable system, thereby reducing the maximum count rate capability of the photon counting system. All PMTs tested produced similar response characteristics to changes in the discriminator's pulse width and voltage thresholds.

The setting of the discriminator threshold of a photomultiplier utilized in a photon counting system is critical in order to maximize the counting system's sensitivity and signal-to-noise response. Each tube was

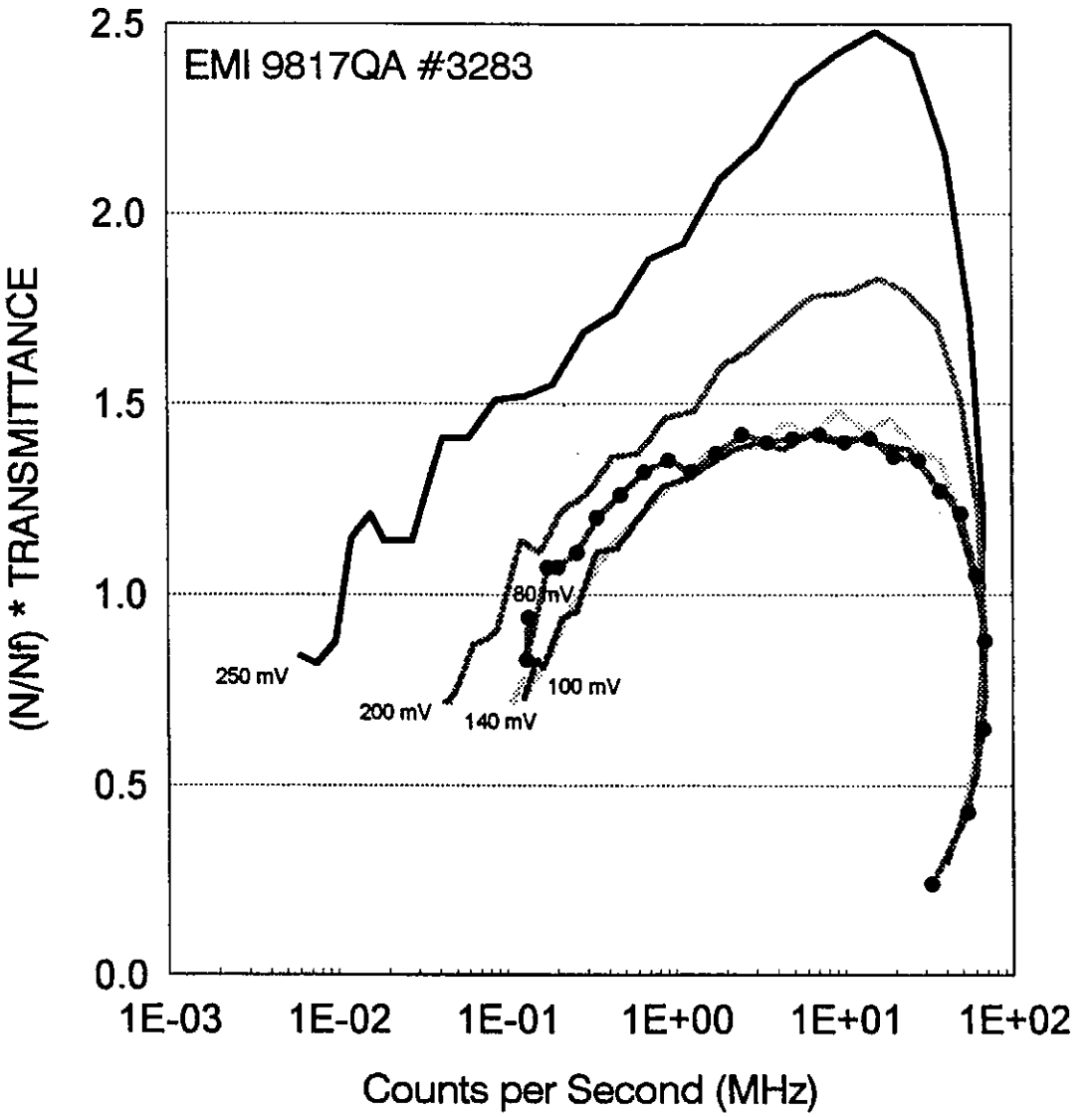

Figure 4.3. Discriminator voltage threshold measurements indicating the nonlinear effects produced by improper threshold settings.

evaluated using the focus grid tube base and magnetic shielding in a light tight configuration. The anode of the PMT was connected to the input of the Phillips Scientific 6950 times ten amplifier. The output of the amplifier was terminated into 50 ohms at the input of the pulse height analyzer (PHA) for pulse height analysis of the selected PMT's dark count response.

Once the PMT was placed into the light tight configuration, cathode voltage corresponding to a gain of 1.5×10^7 was applied and allowed to reach equilibrium (approximately one minute) before conducting the pulse height analysis. Collection times of 0.5, 1.0, 5.0, and 10.0 minutes were selected to collect and chart the pulse height distributions. Pulse height distributions of the 6950 amplifier with no input were also taken during the analysis process. Figure 4.4 displays the pulse height distribution taken after PMT insertion into the measurement setup. The initial pulse distribution is the large source of low voltage noise pulses attributed to amplifier operation and noise generated by the PMT due to exposure to ambient light during the insertion procedure. Following the large distribution of low voltage noise is the pulse distribution of single electron events produced by the PMT photocathode due to exposure to ambient light. Count rate was determined as the total number of counts for a particular voltage divided by the total collection time in

seconds. The incremental PHA measurements were repeated for time intervals of 1, 12, and 24 hours to investigate the expected distribution decrease of single electron events and then to select the desired discriminator threshold which corresponded to the point separating the large low voltage noise distribution from the single electron response of the PMT. The optimum discriminator threshold for a particular PMT was selected by locating the point on the pulse height distribution curve of minimum slope that isolated the transition from low voltage noise and the single electron peak and then drawing a line down from this point to the voltage axis. These measurements are shown in Figure 4.5. As expected, the pulse distribution of the single electron events decreases over time while held in the light tight enclosure. However, the respective decrease in pulse distribution depended upon the individual response characteristics of the PMT under investigation. There were also several cases of increasing single electron pulse distribution which was attributed to thermal heating of the PMT enclosure and tube base components. EMI 9817QA #3233 demonstrated the most significant single electron pulse increase over time. The optimized discriminator thresholds, corresponding to 30 Hz DIAL laser operation, are listed for each PMT in Table 4.1.

4.1.3 Saturation Count Rate

Examining PMT saturation effects are necessary in order

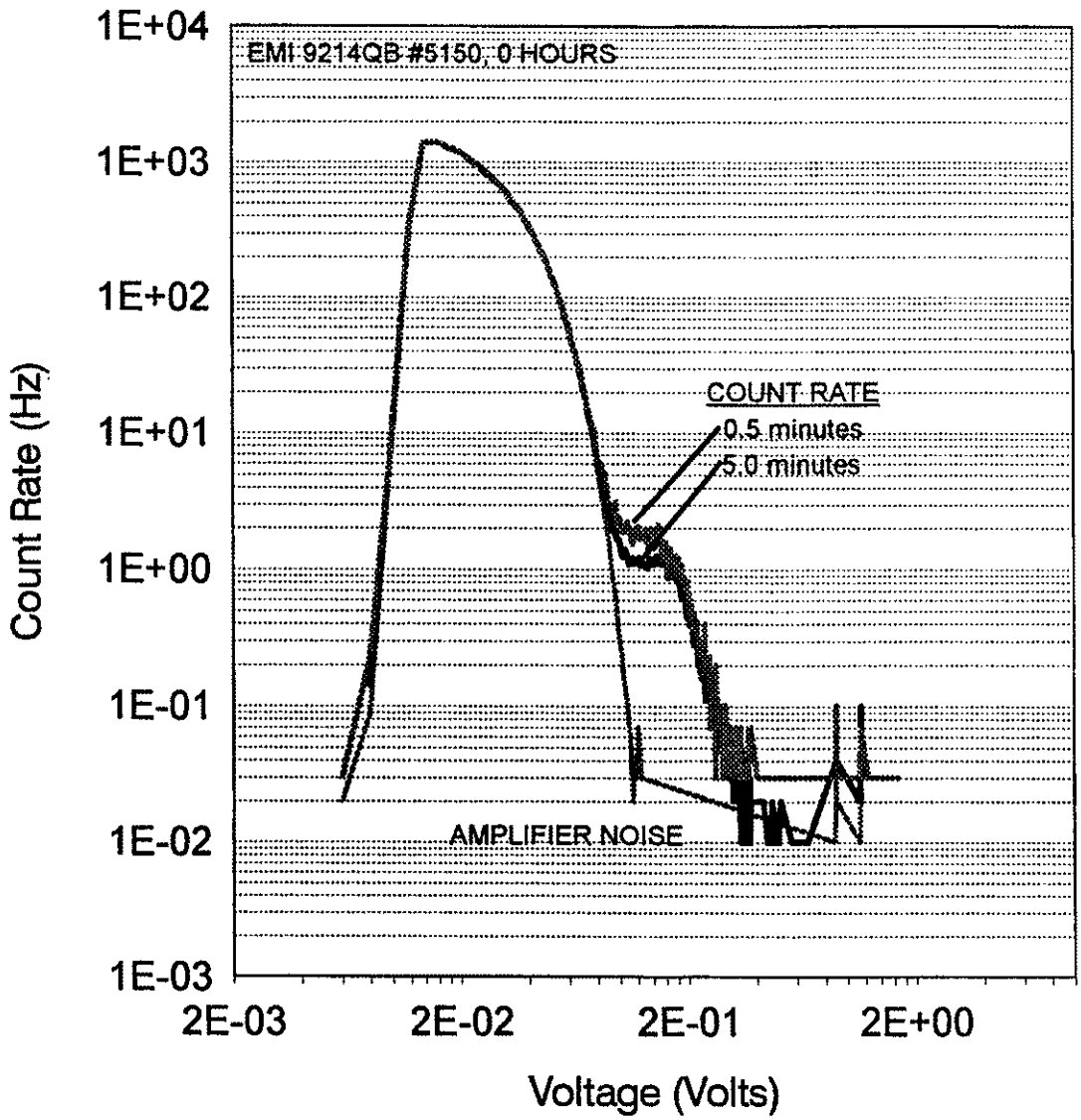

Figure 4.4. Pulse height distribution following photomultiplier tube insertion into the threshold experimental configuration.

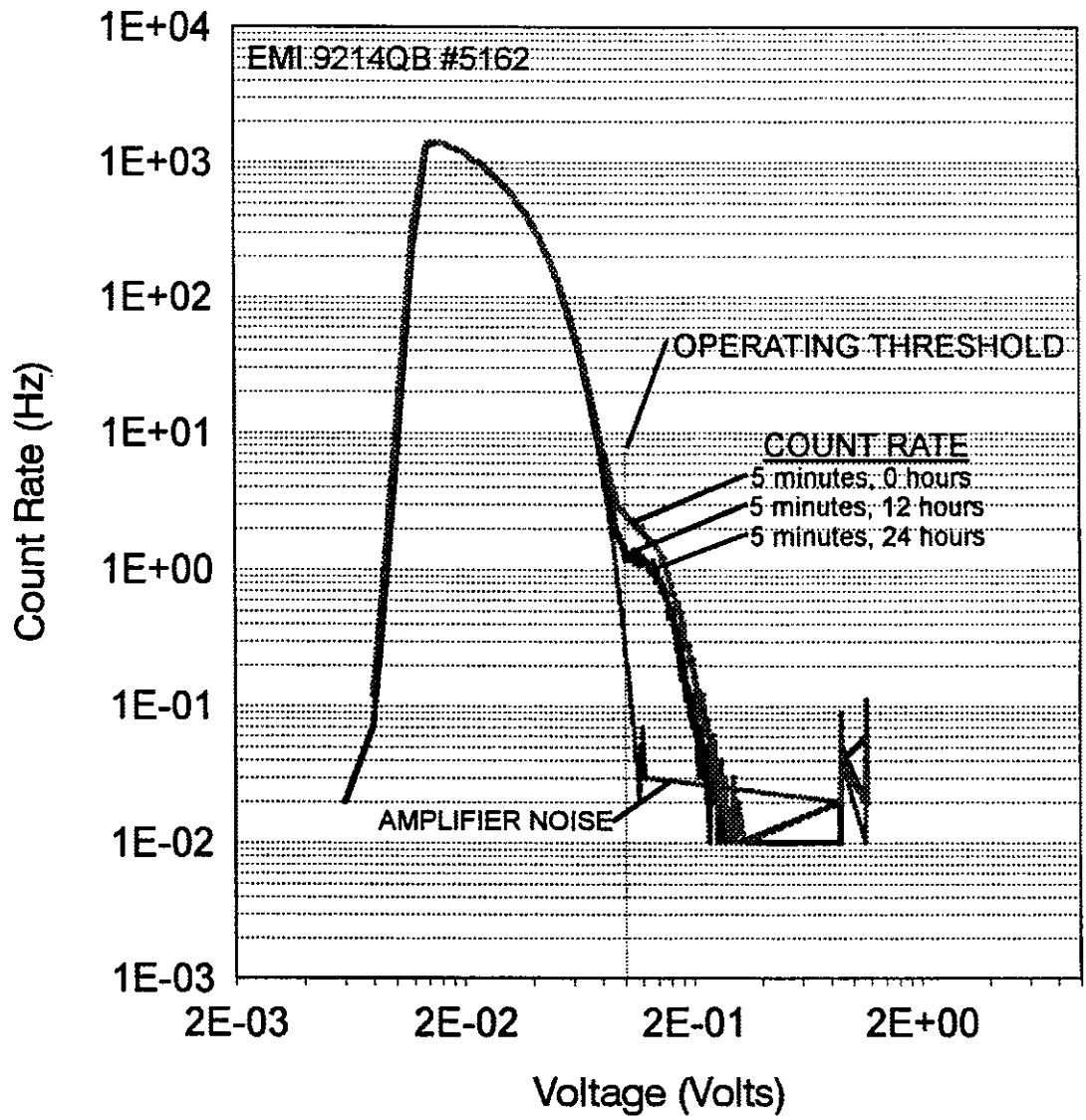

Figure 4.5. Photomultiplier pulse height distributions of incremental PHA measurements investigating the distribution of single electron events with respect to time.

to develop an understanding of the tube's operating limits. Understanding of PMT operation is needed to ensure linear photon counting measurements are taken by the counting system. Saturation of a PMT may be produced by excessive cathode voltages (which causes internal arcing inside the tube) or by exposure to intense incidence light sources. PMT recovery from a saturation condition depends upon the duration and severity of the saturation stimulus and the individual properties of the tube itself.

Saturation effects of PMTs were evaluated using the experimental setup shown in Figure 3.2. The xenon light source was set to 25 amperes and 20 volts DC. Light incident onto the PMT photocathode surface was varied by adjustments of the slit width assemblies. Figure 4.6 shows the measured increase of count rate corresponding to increased light exposure. It is also noted that as the applied PMT cathode voltage is increased an expected increase in count rate also occurs due to the increase of current gain amplifying more noise. As the intensity of light is increased the PMT count rates begin to experience a decrease and eventual roll-off. Photon counting measurements taken at these levels of light exposure would lead to nonlinear responses and should be avoided. As the cathode voltage is increased, saturation of the PMT occurs at lower light intensities due to the increased PMT current

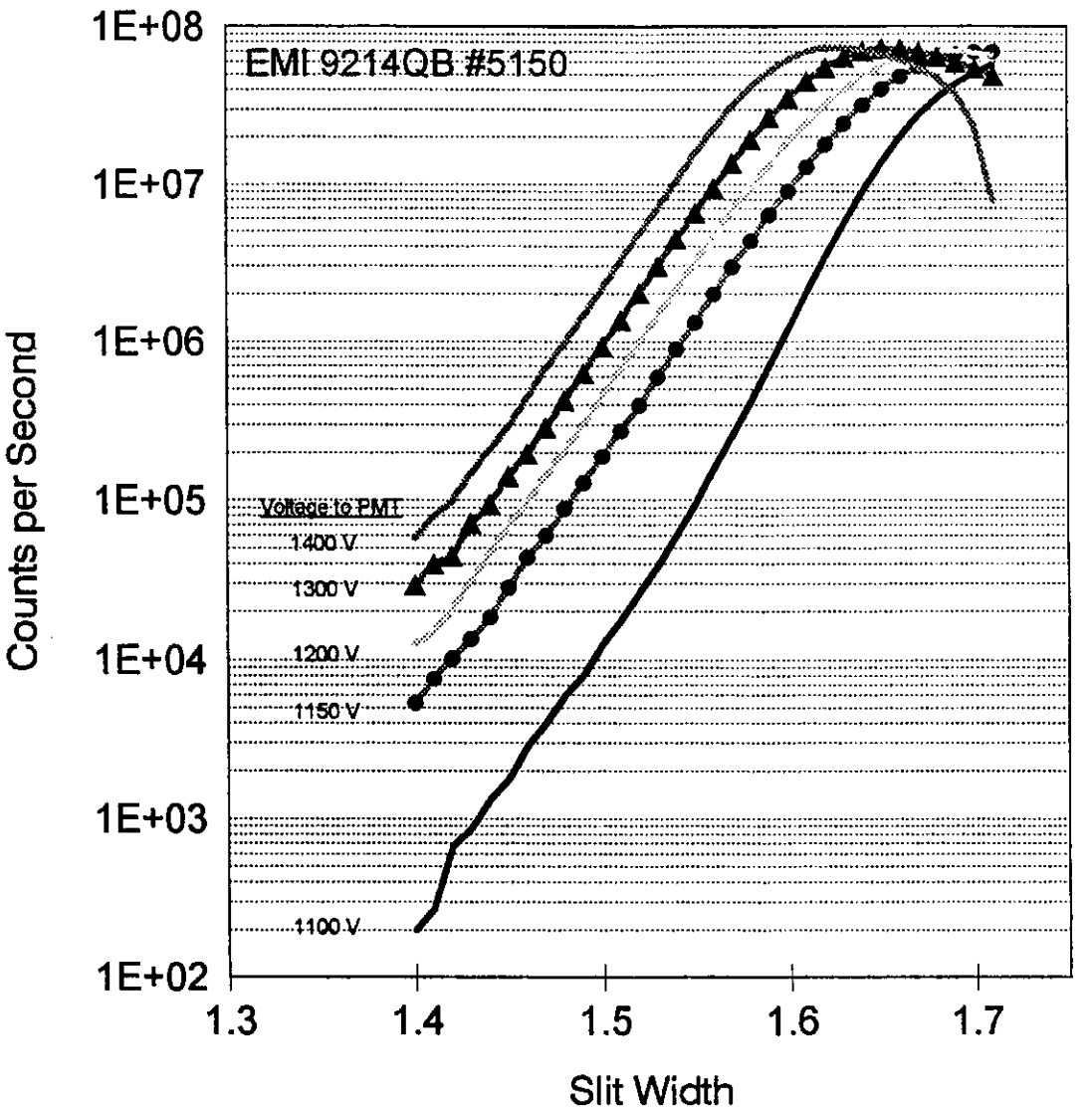

Figure 4.6. Photomultiplier tube saturation data due to increasing light intensities.

gain. All of the PMTs examined produced similar saturation effect responses.

4.1.4 Signal-to-Noise Ratio

Photon counting analysis of the PMT's signal-to-noise ratio (SNR) is necessary in order to identify the PMT cathode voltage range that produces the maximum SNR. Using the experimental setup shown in Figure 3.2, photon counting measurements of signal count rate and dark count rate were taken for a set PMT cathode voltage (at constant 300 nm light intensity). Calculation of the SNR was performed by dividing the measured signal count rate by the measured dark count rate. The selected cathode voltage range for signal-to-noise analysis was covered in increments of 25 volts. The PMT count rate, dark count rate, and SNR results were plotted as shown in Figure 4.7.

The SNR measurements were used to isolate the respective PMT cathode voltage operating values that produced linear count rates and yielded maximum detector SNR values. The linear count rate in Figure 4.7 extends from 1175 to 1475 cathode volts. In this cathode voltage range the corresponding dark counts have a linear response as well. After 1475 volts, dark counts increase nonlinearly and photon counting in this region would lead to unsatisfactory SNR results. Cathode voltage ranges of PMTs that yielded linear SNRs evaluated in the experimental system setup are listed in Table 4.1.

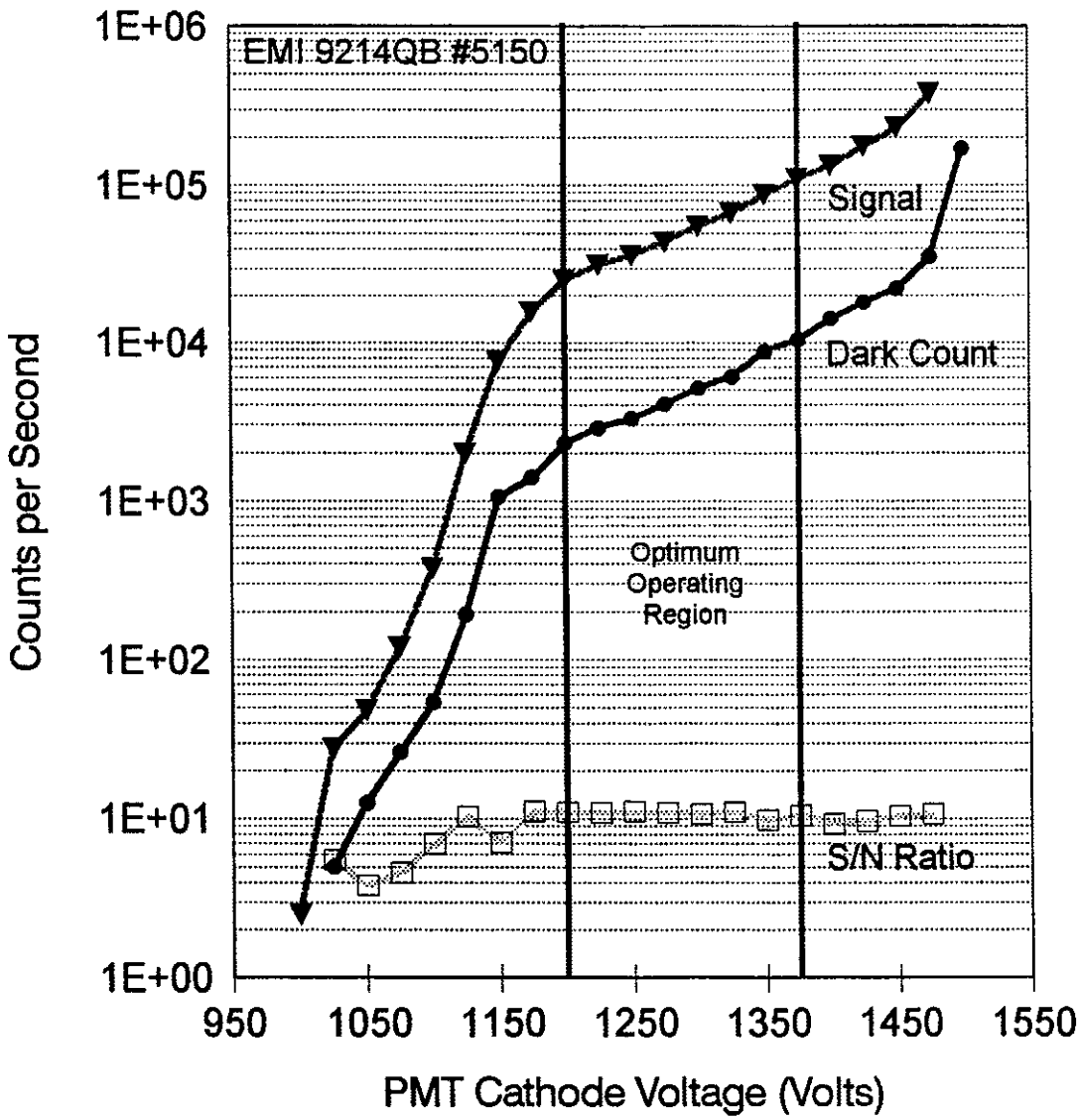

Figure 4.7. Signal-to-noise results shown with photomultiplier tube count rate and dark count rate.

4.1.5 Photomultiplier Tube Linearity

Linearity analysis of the pulsed output of a PMT is necessary to verify proper photon counting system operation and to ensure linear PMT output. As seen in Figure 4.8, if a PMT is exposed to low light intensities at relatively high cathode voltages, significant nonlinearities can be introduced at relatively low PMT output values. The desired PMT linearity response is shown in figure 4.9. At a voltage output of two volts from the PMT and amplifier, the slope and signal change during the gated-on period should be negligible. These requirements are desired because of the differential nature of the lidar DIAL measurement.

Linearity measurements were conducted using the experimental arrangement shown in Figure 3.2. The amplifier output was connected to a 50 ohm load on a digitizing oscilloscope used to display the 1000 sum averaged data of the PMT output. The voltage output of the PMT with amplifier was controlled by varying the light intensity incident on the PMT. Once the desired voltage output was attained (2 volts), the PMT with amplifier output was averaged and printed out for hard copy analysis. The slope and signal change of the voltage outputs were calculated and listed in Table 4.1. The measured PMT output signal changes were quite low and are desired for the DIAL measurement technique. Due to the individual operating characteristics of the PMTs, there was no clear operating linearity

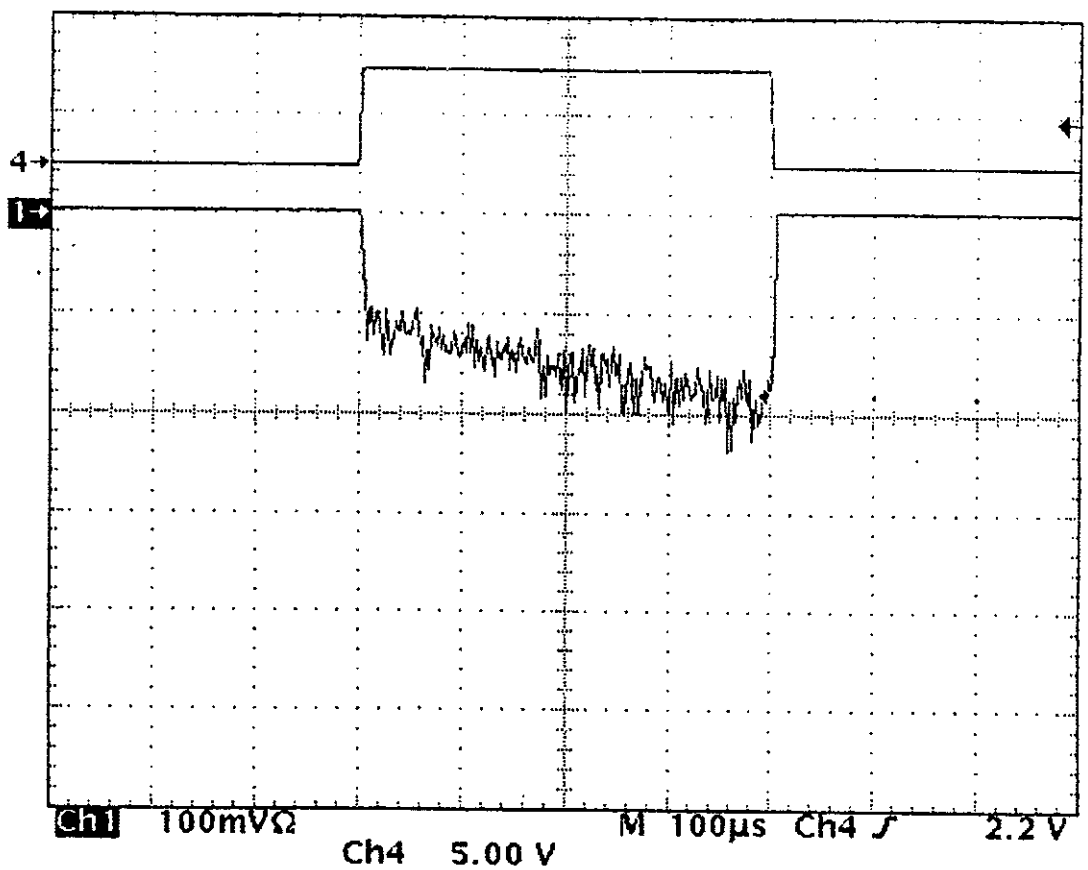

Figure 4.8. EMI 9214QB #5150 at 1500 volts showing nonlinear output during gate on period. Minimal light exposure. Ch 1: Tube output. Ch 4: Gate signal.

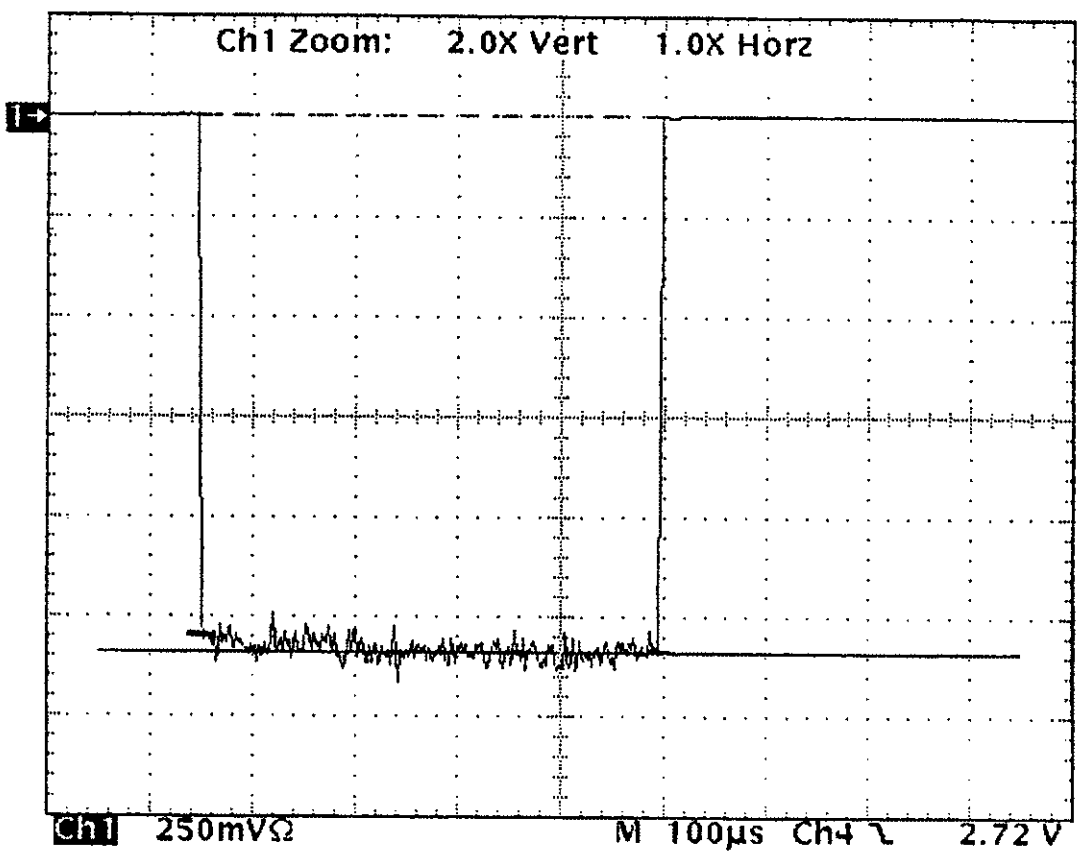

Figure 4.9. EMI 9817QA #3236 at 2300 volts showing typical linear output. Ch 1: Tube output.

difference between the EMI 9214Q and EMI 9817Q series. PMTs EMI 9214QB #5162 and EMI 9817QA #3236 produced the best linear response during the gate on period.

4.2 Photomultiplier Tube Base Gating Comparisons

The focus grid and four dynode gating designs (see Figures 3.4 and 3.5) were investigated to evaluate the PMT holdoff characteristics. Holdoff describes the ability of a base gating circuit to effectively prevent high intensity ultraviolet light bleedthrough through the PMT when the gate is turned off. In the present experimental setup, a PMT is continuously exposed to ultraviolet light. Thus, the PMT's photocathode is continuously releasing photoelectrons that would result in unwanted pulse signals or undesirable ultraviolet light bleedthrough. Holdoff is a ratio of the gated-on current of the PMT to the gated-off current for a particular cathode voltage setting and input light intensity. A low holdoff value allows for generation of unwanted signal pulses (near field aircraft lidar return). If the PMT is highly saturated during the gated-off period, it may not operate in a linear fashion when the gate is turned on.

The focus grid gating design produces a zero voltage difference between the photocathode and the focus grid during the gated-off period turning off the PMT while exposed to lidar returns. When the PMT was gated-on, a potential difference develops between the photocathode and

focus grid allowing the buildup of electrons on the photocathode to accelerate through the dynode chain. Another source of unwanted signal in the gated-off condition is the generation of electrons by ultraviolet light passing through the photocathode and focus grid striking the surface of the first dynode in the amplification chain liberating electrons. Values of photocathode ultraviolet light transparency for EMI 9214Q and EMI 9817Q are 37% and 14% respectfully. These dynode electrons are amplified by the rest of the dynode chain which result in signal generation even when the focus grid is biased off.

The four dynode gating circuit is designed to reduce the generation of signal current due to the incident ultraviolet light while in the gated-off condition. With the PMT gated-off, four dynodes are electrically turned off blocking the amplification of charge on the photocathode. Another benefit to this design is that electrons generated by ultraviolet light incident upon the first dynode, in a gated-off condition, are not permitted to continue through the dynode chain and do not result in unwanted signal current anomalies. The disadvantages associated with the four dynode gating circuit design are the need to optimize the values of the variable resistors (R1, R2, and R3) and for the need of a high pulsed gate voltage. However, once these values were determined they remain constant for a particular PMT.

The holdoff measurements were performed in the PMT measurement system shown in Figure 3.2. The xenon light source was adjusted to 25 amperes and 20 volts DC. The amount of 300 nm light exposed to the PMT was set by varying the slit widths of the variable slit assemblies to obtain a 2.00 volt averaged output from the PMT with amplifier terminated with a 50 ohm load. The maximum PMT cathode voltage was used for this light adjustment to prevent any nonlinear effects while conducting the holdoff measurements over the selected PMT cathode voltage range. The holdoff measurements for the selected PMT and gating design were conducted by allowing a selected cathode voltage to reach an equilibrium condition (approximately 1 minute). The applied gate voltage should also be adjusted to optimized gate voltage for the respective cathode voltage. With a gate signal applied, a 1000 averaged sample was taken of the PMT output voltage while exposed to the 300 nm light source. The gate signal was then disconnected and the anode of the PMT was connected to a digital photometer. Current output from the PMT, while exposed to the 300 nm light source, was measured by the photometer and used to calculate the holdoff ratio of gated current to non-gated current. These steps were repeated for the PMT's allowed cathode voltage range. The four dynode gating photomultiplier's holdoff data is plotted and shown in Figure 4.10. Also shown in Figure 4.10 is the optimized gate voltage for the corresponding cathode

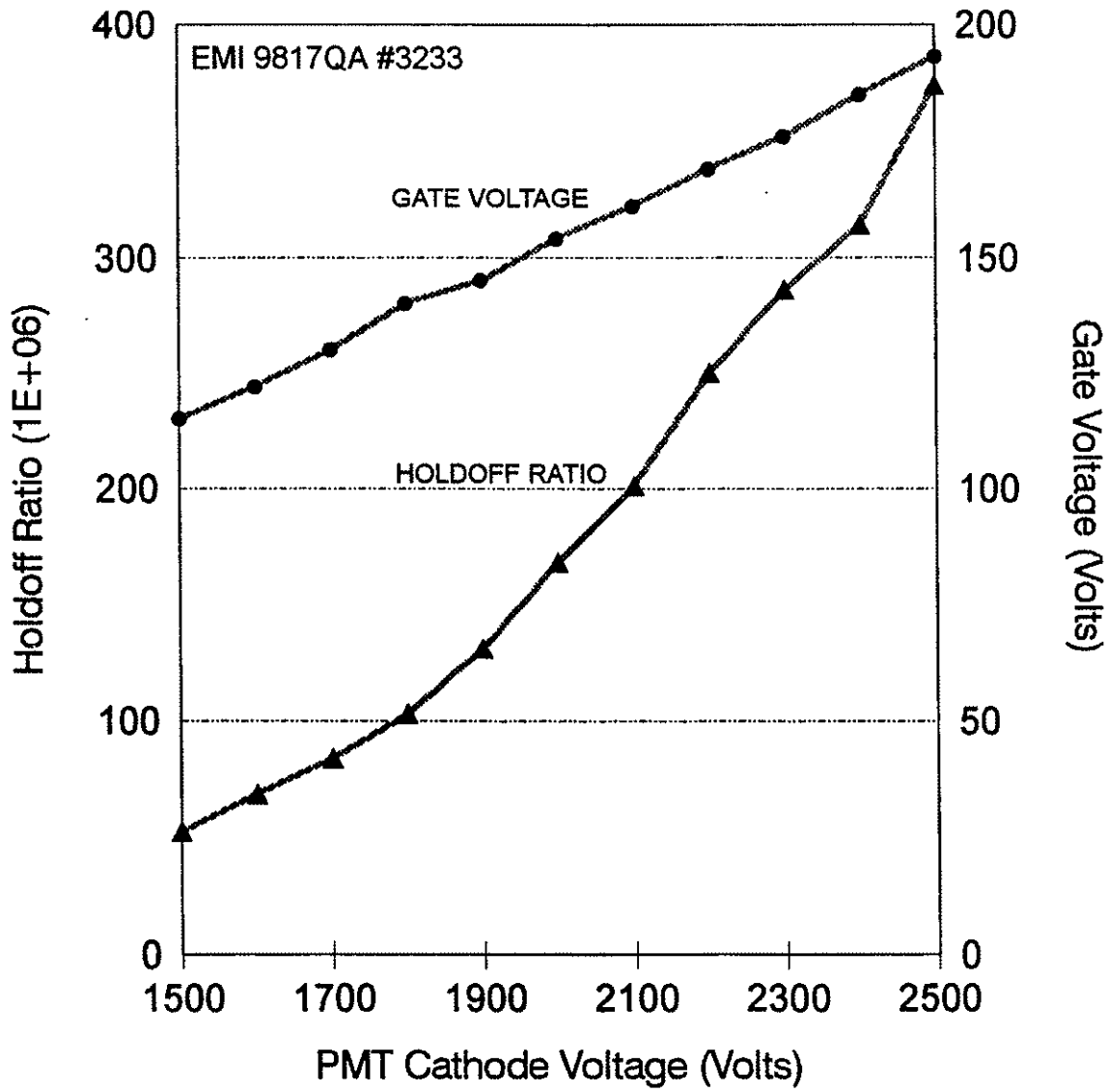

Figure 4.10. Four dynode gating photomultiplier tube holdoff data with corresponding gate voltage for linear pulsed output.

voltage. The holdoff characteristic of the four dynode gating design was superior to that of the focus grid design. The measured holdoff of the four dynode gating design yielded a maximum ratio of 3.7×10^8 for the EMI 9817QA #3233 PMT compared to a maximum of 6.3×10^4 for the focus grid gating scheme. The holdoff characteristics attained with the four dynode gating design were on average 1000 times higher than that achieved by the focus grid gating configuration. Another point of interest is that as the cathode voltage was increased the holdoff ratios of the four dynode design increased while the focus grid system's holdoff values decreased.

4.3 Photon Counting Lidar Ozone Measurements

In order to validate the lidar ozone measurements gathered by the photon counting system, differential absorption lidar returns were collected independently by the photon counting and analog detection systems. Night measurements were conducted during the month of November, 1996. The ozone DIAL signal processing system provided both detection schemes with the required external trigger (30 Hz) and clock signal (1 MHz). The PMT gate signal was applied in concurrence with the external trigger. This gate signal consisted of two 250 μsec pulses separated by 25 μsec and represented the on-line and off-line ozone return signals, respectively. The photon counting system's multichannel analyzer was programmed to collect 550 dwell periods of data

which provided adequate coverage of the applied gate signal. A collection time of 30 seconds was used for both systems. This collection time corresponded to 900 system laser shots.

The PMT selected for the ozone measurements was the EMI 9214QB #5150. This particular PMT provided the highest quantum efficiency in the ultraviolet region (31.5% at 300 nm), minimal dark counts, relatively low cathode voltage for the desired gain (1.5×10^7 gain at 1300 volts DC), and negligible nonlinear output signal distortion. The focus grid gated tube base was used to distribute the applied cathode voltage due to familiarity with the component operating characteristics. Discriminator setpoints corresponded to the optimum settings for the EMI 9214QB #5150 PMT. A discriminator pulse width of five nanoseconds minimized the effect of pulse pile-up errors and provided the maximum linear operating response. The ideal discriminator threshold voltage was determined to be 110 mV, which thereby restricted the introduction of low voltage noise counts in the photon counting analyses.

Data collected by the photon counting and analog detection systems was deposited into their respective computer memory systems in a sequential manner. The first 30 second collection period was performed by the analog system. Upon completion of the analog system collection period, the photon counting system initiated its collection sequence and stored its data in an appropriate data file.

This process was repeated to obtain the required ozone validation data. Once the nightly data sequences had been completed, the respective computer programs processed the collected ozone data.

The photon counting data was entered into Equation (5) to calculate the measured ozone density (m^{-3}) with respect to altitude (km). For Equation (5), the range interval corresponded to 60,000 cm or four dwell periods. The differential ozone absorption cross-section for the operating on- and off-line laser wavelengths corresponded to 1.19×10^{-18} cm^2. The respective collection periods were averaged together and resulted in the averaged ozone number density profile. Measured ozone densities of 10^{18} m^{-3} correspond to an ozone mixing ratio of 37 parts in 10^9, volume (ppbv) [12]. The results of the photon counting and analog averaged ozone profiles can be seen in Figure 4.11.

As shown in Figure 4.11, the photon counting and analog ozone profiles produced similar results. The theoretical upper ozone detection range, based upon the gate signal pulse width of 250 μsec, was expected to be 37.5 km. However, due to the winter atmospheric conditions (lower tropospheric and stratospheric ozone distributions) and effects of low lying clouds, the actual detection range was much less at approximately 15 km. The effects of low lying clouds can be seen in the 1.2 to 3 km range, as both detection methods are subject to increased lidar laser

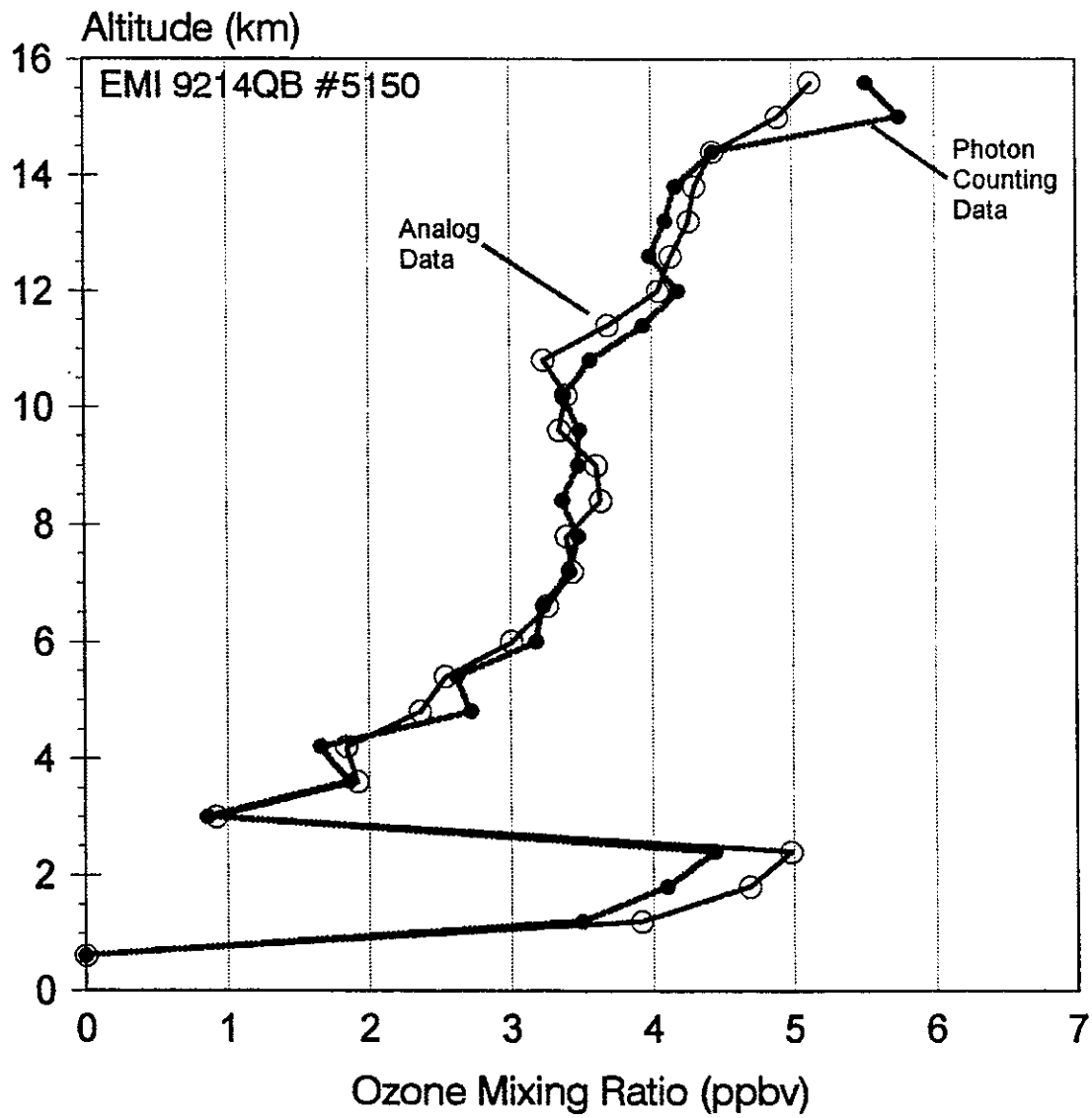

Figure 4.11. Comparison of average ozone profiles for photon counting (solid dots) and analog (open dots) lidar return signals.

backscattering. Beyond three kilometers, both systems illustrate the predicted tropospheric increase of ozone density with increasing altitude as shown in Figures 1.1 and 1.2. The photon counting and analog data points were in good agreement with an overall difference of 6.1 percent. The maximum difference in data point values was found at 15 and 4.8 km (17.3 and 15.3 percent, respectively), with photon counting producing the higher counts. These night ozone measurements produced the necessary data to establish the photon counting system as a analogous ozone detection method against the current analog system.

CHAPTER V

SUMMARY AND CONCLUSIONS

5.1 Photomultiplier Tube Test Results and Selection

Analysis of each photomultiplier tube was necessary for proper determination of operating characteristics required for photon counting. Each PMT of the same series and manufacturer will have unique and occasionally undesirable response attributes. Preselected current gains allowed for proper evaluation of PMT noise count rate, saturation count rate, signal-to-noise ratio, linearity, and discrimination threshold and pulse width. Also, PMT properties such as quantum efficiency and low cathode voltage for dictated gain were considered. PMT test results are summarized and listed in Table 4.1.

The EMI 9214Q PMT series was selected as a replacement for the EMI 9817Q PMT series to conduct lidar ozone detection. The EMI 9214Q series, in general, provided higher quantum efficiencies in the ultraviolet values of interest (289-311 nm). This series of PMTs also reduced the necessary cathode voltage for related tube gain by roughly a factor of two. This operational feature, along with the use of CsSb dynode chain material, accounts for the decrease in noise count rate by a factor of greater than ten over the EMI 9817Q series. Discriminator pulse width settings should be maintained at a minimum in order to lessen the effects of

pulse pile-up (in this case, 5 nsec). The EMI 9214Q series allowed for lower discriminator threshold settings and, therefore, increased photon counts. The photomultiplier tube chosen for photon counting measurement was the EMI 9214QB #5150 due to its high quantum efficiency, minimal dark count rate, low cathode voltage, and minimal nonlinear output signal distortion.

5.2 Photomultiplier Tube Base Gating Test Results

The photomultiplier tube base gating networks, focus grid and four dynode gating, tested in the above described experiments performed the proper distribution of applied high voltage DC power to individual PMT dynodes. However, to improve the performance of the ozone measurement system, it proved necessary to optimize distribution of the high voltage DC power in order to enhance PMT operation and output parameters.

Improved PMT performance was obtained through institution of the four dynode gating design. This gate design increased the holdoff characteristic of a selected PMT by a factor of 1000 over the currently used focus grid gating design. Holdoff provided by the four dynode gating design provided an added benefit as it tended to increase with increasing DC power. This is a desired operational attribute, as it is common practice during inflight measurements to increase the PMT's DC power in order to increase the PMT's signal gain.

The four dynode gating design also improved the linearity of PMT output. This improved linearity was obtained by judicious selection of gate voltage with respect to PMT cathode voltage. Once the gate voltage was adjusted to achieve the desired linear PMT output, it remained unique for the selected PMT at that particular PMT cathode voltage. Photomultiplier linearity was also controlled by settings of the variable resistors R1, R2, and R3. Again, once the proper settings of these resistors were determined in a laboratory environment, they remained as constants for the selected PMT and did not require further field adjustments. Thus, the four dynode gating design added to the overall complexity of the ozone detection system but the operational benefits obtained far outweighed the slight increase in laboratory system testing.

5.3 Photon Counting Ozone Measurements

With successful ground ozone data validation of the photon counting system against the current analog detection system, integration of the independent photon counting system into the current DIAL signal detection system is required. This integration of detection systems will allow the photon counting data processing components to take advantage of existing computer processing capabilities employed by the current DIAL signal detection system. This will lead to improved field analysis and increased photon counting data averaging. Once the assimilation is complete,

actual airborne photon counting measurements will be possible. Due to the relatively low operating laser powers (50 mJ) and small diameter telescope receivers (36 cm), ground based ozone measurements are limited to 15 to 20 km under optimum atmospheric conditions.

Future improvements for the photon counting system involve replacing the single level discriminator with an upper and lower level discriminator and further PMT testing under operating conditions. Use of the upper and lower level discriminator would allow for the discrimination of high energy photons generated by cosmic radiation and PMT radioactive contaminates. The added level of discrimination would improve the photon counting system's signal-to-noise ratio for a selected cathode voltage and also improve the ozone count precision.

BIBLIOGRAPHY

[1] R. W. Engstrom, *Photomultiplier Handbook*, (RCA, 1980).

[2] W. Demtroder, *Laser Spectroscopy Basic Concepts and Instrumentation*, (Springer-Verlag, Berlin, 1996).

[3] N. S. Higdon, E. V. Browell, P. Ponsardin, B. E. Grossmann, C. F. Butler, T. H. Chyba, M. N. Mayo, R. J. Allen, A. W. Heuser, W. B. Grant, S. Ismail, S. D. Mayor, and A. F. Carter, "Airborne differential absorption lidar system for measurements of atmospheric water vapor and aerosols," Appl. Opt. **33**, 6422-6438 (1994).

[4] E. V. Browell, A. F. Carter, S. T. Shipley, R. J. Allen, C. F. Butler, N. N. Mayo, N. H. Siviter, Jr., and W. M. Hall, "NASA multipurpose airborne DIAL system and measurements of ozone and aerosol profiles," Appl. Opt. **22**, 522-534 (1983).

[5] C. Jackman and M. Odell, "Ozone: What is it, and why do we care about it?," NASA Facts, The Mission to Planet Earth Series, (Goddard Space Flight Center, Greenbelt, MD, 1993).

[6] J. S. Wager, "Double Exposure," Nucleus **17**, 1-3 (1995).

[7] L. van Bree, M. Marra, H. J. van Scheindelen, P. H. Fischer, S. de Loos, E. Buringh, and P. J. Rombout, "Dose-effect models for ozone exposure: tool for quantitative risk estimation," Toxicol. Lett. **82-83**, 317-321 (1995).

[8] E. E. Uthe, J. M. Livingston, and N. B. Nielsen, "Airborne lidar mapping of ozone concentrations during the Lake Michigan ozone study," J. Air Waste Manage. Assoc. **42**, 1313-1318 (1992).

[9] "Optech awarded contract for lidar to monitor polar stratosphere," Air & Waste **44**, 812-813 (1994).

[10] U. Kempfer, W. Carnuth, R. Lotz, and T. Trickl, "A wide-range ultraviolet lidar system for tropospheric ozone measurements: development and application," Rev. Sci. Instrum. **65**, 3145-3163 (1994).

[11] O. Uchino and I. Tabata, "Mobile lidar for simultaneous measurements of ozone, aerosols, and temperature in the stratosphere," Appl. Opt. **30**, 2005-2012 (1991).

[12] J. A. Sunesson, A. Apituley, and D. P. Swart, "Differential absorption lidar system for routine monitoring of tropospheric ozone," Appl. Opt. **30**, 7045-7058 (1994).

[13] E. V. Browell, C. F. Butler, M. A. Fenn, W. B. Grant, S. Ismail, M. R. Schoeberl, O. B. Toon, M. Loewenstein, and J. R. Podolske, "Ozone and aerosol changes during the 1991-1992 airborne arctic stratospheric expedition," Science **261**, 1155-1158 (1993).

[14] *U. S. Standard Atmosphere, 1976*, (National Oceanic and Atmospheric Administration, National Aeronautics and Space Administration, and United States Air Force, 1976).

[15] *Photomultipliers and Accessories*, (THORN EMI Electron Tubes, Middlesex, England, 1993).

[16] G. H. Rieke, *Detection of Light: from the Ultraviolet to the Submillimeter* (University Press, Cambridge, 1994).

[17] M. L. Meade, "Instrumentation aspects of photon counting applied to photometry," J. Phys. E: Sci. Instrum. **14**, 909-918 (1981).

[18] B. H. Candy, "Photomultiplier characteristics and practice relevant to photon counting," Rev. Sci. Instrum. **56**, 183-192 (1985).

[19] "Photon Counting-What is it?", 11-20 (Stanford Research Systems, Sunnyvale, CA, 1994).

[20] D. P. Donovan, J. A. Whiteway, and A. I. Carswell, "Correction for nonlinear photon-counting effects in lidar systems," Appl. Opt. **32**, 6742-6753 (1993).

[21] E. V. Browell, "Differential absorption lidar sensing of ozone," Proceedings of the IEEE **77**, 419-432 (1989).

[22] E. V. Browell, "Airborne Lidar Measurements," Rev. Laser Eng. **23**, 135-141 (1995).

[23] M. H. Proffitt and A. O. Langford, "Profiling of Ozone in the Free Troposphere by the lidar Technique," Rev. Laser Eng. **23**, 104-107 (1995).

[24] E. V. Browell, S. Ismail, and S. T. Shipley, "Ultraviolet DIAL measurements of O_3 profiles in regions of spatially inhomogeneous aerosols," Appl. Opt. **24**, 2827-2836 (1985).

[25] R. M. Schotland, "Errors in the lidar measurement of atmospheric gases by differential absorption," J. Appl. Meteor. **13**, 71-77 (1974).

[26] A. I. Carswell, S. R. Pal, W. Steinbrecht, J. A. Whiteway, A. Ulitsky, and T. Y. Wang, "Lidar measurements of the middle atmosphere," Can. J. Phys. **69**, 1076-1086 (1991).

[27] J. D. W. Barrick, "Gating characteristics of photomultiplier tubes for lidar applications," NASA Tech. Mem. 87699 (Langley Research Center, Hampton, VA, 1986).

[28] M. P. Bristow, D. H. Bundy, and A. G. Wright, "Signal linearity, gain stability, and gating in photomultipliers: application to differential absorption lidars," Appl. Opt. **34**, 4437-4452 (1995).

[29] H. S. Lee, G. K. Schwemmer, C. L. Korb, M. Dombrowski, and C. Prasad, "Gated photomultiplier response characterization for DIAL measurements," Appl. Opt. **29**, 3303-3315 (1990).

[30] *Model 2190 Multichannel Scaling Averager Technical Sheet*, (DSP Technology Inc., Fremont, CA, 1988).

[31] *LH 151N Lamphousing Instruction Manual*, (Kratos Analytical Instruments, Ramsey, NJ, 1991).

[32] *Stanford Research Systems 1996-97 Scientific and Engineering Instruments*, (Stanford Research Systems, Sunnyvale, CA, 1996).

APPENDIX A

PHOTON COUNTING COMPUTER PROGRAM

This Visual C++ program controls the operation sequence of a CAMAC based photon counting system. The output of the PMT with amplifier provides the input signal to the CAMAC powered pulse height discriminator. The discriminator sends its pulsed output to the DSP 2190 multichannel analyzer (DSP 2190 is physically composed of two interconnected modules, a DSP 2090S high speed scaler and a DSP 4101 high speed averaging memory). The collected data and module commands are relayed through a LeCroy 8901A CAMAC to GPIB interface module. A 486 computer, which houses the NI-488.2 MS-DOS software and hardware, generates the program command sequence based on the user input data. The photon counting program is executed by entering the executable file, DSP 4101 slot number, number of sweeps, and record length. Commands are then issued to clear and initialize the multichannel analyzer with the input data and to open the output file. Pulse counting is enabled and continues until the number of sweeps is completed. An external trigger and dwell signal is provided to the DSP 4101 module by the master control system. Finally, the data read command is issued to read the signal averaged data and to store the collected data into an output file for further analysis.

```
// Link this program with mcib.obj.

#include <stdlib.h>
#include <string.h>
#include <stdio.h>
#include <time.h>
#include "decl.h"

int bd;                    //IEEE board number

//function prototypes
void finderr(void);
void error(void);
void send_cmd(int f, int a, int sta_nu);
void send_cmd_dat
   (int f, int a, int sta_nu, int dat1, int dat2, int dat3);
void read_dat2 (char *mmrd);

//begin main program
void main(int argc, char **argv)
{
 char *rd;                 //data pointer
 int Q = 1;                //indicates valid data transfer
                           // (1), or end of data transfer (0)
 int count = 0;            //number of data sweeps
 FILE *fp;                 //output file pointer
 int swp_nu;               //number of sweeps
 int rcd_len1, rcd_len2;   //record length, stored in two
                           // words
 int swp_nu1, swp_nu2;     //number of sweeps, stored in two
                           // words
 int sta_nu;               //CAMAC station number
 double nu_rd;             //output data words that are read
 double total_counts = 0;      //total number of photon
                               // counts of interval
 static char tmpstr[8];        //temporary storage array
 int i;                        //loop control variable
 double sec_wait;              //time delay variable
 long temp;                    //temporary data variable

 fp = fopen("abcde", "w");     //open output files

 printf("\nLeCroy 8901A & DSP 2190 control program.\n");

 //test for proper entry of data from DOS prompt
 rd = (char*)malloc(5);
 if(argc != 5)
   { printf("Usage: DSP4101 [station #] [# of sweep]");
     printf(" [record length] [sec to wait]\n");
     exit(1);
   }
```

```
//initialize interface components
if((bd = ibfind("GPIB0")) < 0) finderr();
                        //identifies IEEE card interface
if(ibtrap(ERR, 3) & ERR) error(); //calls appmon error
                                  // program
if(ibsic(bd) & ERR) error();      //send interface clear,
                                  // initializes the GPIB
if(ibsre(bd, 1) & ERR) error();   //set(1) or clear(0) the
                                  // remote enable line

send_cmd(100, 0, 0);     //CAMAC LeCroy Interface, four word
                         // return
send_cmd( 9, 0, 12);     //2090, reset module, zero scaler
send_cmd(24, 0, 12);     //2090, disable the CAMAC dataway
                         // LAM

sta_nu = atoi(argv[1]); //4101 station number assignment
sec_wait = (double) atof(argv[4]); //time delay assignment

rcd_len1 = 0x00ff & atoi(argv[3]);     //record length
                                       // assignment
rcd_len2 = 0xff00 & atoi(argv[3]);
rcd_len2 >>= 8;
rcd_len2 &= 0x00ff;

swp_nu = 0xffff - (atoi(argv[2]) - 1); //number of sweeps
                                       // assignment
swp_nu1 = swp_nu & 0x00ff;
swp_nu2 = swp_nu & 0xff00;
swp_nu2 >>= 8;
swp_nu2  &= 0x00ff;
send_cmd(24, 1, 13);     //4101, disable averaging
                         // generates internal LAM
send_cmd_dat(16, 2, 13, 0, 0, 0); //4101, writes the
                                  // control status
send_cmd_dat(16, 3, 13, rcd_len1, rcd_len2, 0);
                         //4101, sets the record length
send_cmd_dat(17, 0, 13, swp_nu1, swp_nu2, 0);
                         //4101, sets the sweeps register
send_cmd(26, 1, 12);     //2090, enables counting
send_cmd( 9, 0, 13);     //4101, resets the module, clears
                         // memory to zero,enables averaging
send_cmd(26, 0, 13);     //4101, enables LAM, moved for
                         // operation with 8901A

send_cmd_dat(16, 1, 13, 1, 0, 0); //writes address of first
                                  // data word to be read
                                  // from the averaging
                                  // memory

send_cmd( 2, 0, 13);     //reads the signal averaged
                         // waveform data
```

```
while(Q == 1)                    //data reading loop
  { read_dat2(rd);
    if((rd[3] & 0x02) == 0x00) {Q = 0; break;}
                                 //end loop after all data has
                                 // been recorded
    nu_rd = rd[0] & 0x00ff;
    temp = rd[1] & 0x00ff;
    nu_rd += (temp << 8);
    temp = rd[2] & 0x00ff;
    nu_rd += (temp << 16);
    count++;                     //number of data sweeps
    total_counts += nu_rd;       //sum of photon events
    printf("nu_rd _x:%4x    \t", (long)nu_rd);
                                 //individual bin photon events
    printf("_d:%.f\n", nu_rd);
    fprintf(fp,"%d\t%.f\n", count, nu_rd);
                                 //stores data in output files
  }

printf("count = %d\n",count);
printf("total counts =  %.f", total_counts);

send_cmd(10, 0, 13);     //resets the LAM

ibsic(bd);               //sends interface clear,
                         // initializes the GBIP
ibonl(bd,0);             //places interface board offline
fclose(fp);              //closes output file
exit(0);
}


////////////////////////////////////////////////////////////
void finderr(void)
{
 printf("Ibfind error; can't find device or board\n");
 exit(1);
}

////////////////////////////////////////////////////////////
void error(void)
{
 printf("GPIB function call error:\n");
 printf("ibsta = 0x%x, iberr = 0x%x, ibcnt = 0x%x\n");
 printf(ibsta, iberr, ibcnt);
 exit(1);
}

////////////////////////////////////////////////////////////
void send_cmd(int f, int a, int sta_nu)
{
 static char tmpstr[4];
```

```
 ibcmd(bd, "?_!@", 4);
 if (ibsta & ERR) error();
 sprintf(tmpstr, "%c%c%c", f, a, sta_nu);
 ibwrt(bd, tmpstr, 3);
 ibcmd(bd, "A", 1);
 if (ibsta & ERR) error();
}

////////////////////////////////////////////////////////////
void send_cmd_dat
     (int f, int a, int sta_nu, int dat1, int dat2, int dat3)
{
 static char tmpstr[7];

 ibcmd(bd, "?_!@", 4);
 if (ibsta & ERR) error();
 sprintf(tmpstr, "%c%c%c%c%c", f, a, sta_nu, dat1, dat2);
 sprintf(dat3);
 ibwrt(bd, tmpstr, 6);
 ibcmd(bd, "A", 1);
 if (ibsta & ERR) error();
}

////////////////////////////////////////////////////////////
void read_dat2(char *mmrd)
{
 ibcmd (bd, "?_A ", 4);
 if (ibsta & ERR) error();
 if (ibrd(bd, mmrd, 5) & ERR) error();
 return;
}
```

APPENDIX B

SNUBBING SIGNAL RECOVERY RESULTS

Signal recovery experiments were conducted to evaluate the photon counting system response to a snubbing network connected to the PMT anode. The purpose of the snubbing network is to improve the shape of the output pulse for photon counting. However, this circuit will also introduce output signal attenuation. A snubbing network is intended to: 1)reduce pulsed signal fall times, thus, improving pulse pair resolution, 2)cancel excessive pulse ringing that may introduce multiple counts from a single photon event, 3)terminate reflections between the anode output and amplifier input, and 4)prevent charging of the signal cable [27]. Design of the snubbing network consisted of a ten inch piece of 50 ohm RG174/U coax cable which was terminated into a 50 ohm potentiometer (signal round trip time of five nsec).

Utilizing the photon counting experimental setup and a very low intensity 300 nm light input, the snubbing network was connected to the PMT anode which was terminated into a 50 ohm load of a digitizing oscilloscope for photon pulse signal analysis. A typical photon response, without the snubbing network attached, is shown in Figure B.1. The pulse has a relatively short pulse width (4.4 nsec) and rise/fall times. Pulse ringing is evident in Figure B.1 but is not considered significant. Figure B.2 shows a snubbed

pulse output corresponding to a 50 ohm potentiometer setting. Some signal attenuation is evident. The output pulse has also experienced the expected reductions in pulse width (4.4 nsec in Figure B.1 versus 3.6 nsec as noted in Figure B.2) and rise/fall times (4.4 nsec/3.2 nsec in Figure B.1 versus 2.8 nsec/3.2 nsec as shown in Figure B.2). An apparent reduction of pulse ringing life-time is also noted. However, the amplitude of the pulse ringing has been increased. Further reduction in the 50 ohm potentiometer resistance produced more signal pulse attenuation and no additional pulse shaping enhancements. Signal attenuation, due to integration of the snubbing network, was more apparent in photon counting measurements. Count rates suffered a 7 to 38 percent reduction of photon events detected when the snubbing network was in place.

The results of the snubbing circuit were as follows: 1)some signal attenuation; photon counting count rate measurements were reduced by 7-38 percent, 2)reduction of the number of ringing periods, 3)amplitude increases in ringing pulses, 4)reduction of pulse rise time; reduced pulse width, and 5)added noise to amplifier output bias signal. The snubbing network did result in some signal recovery improvements, but these improvements were not significant enough compared to the signal attenuation and thus was not incorporated into the photon counting measurement setup.

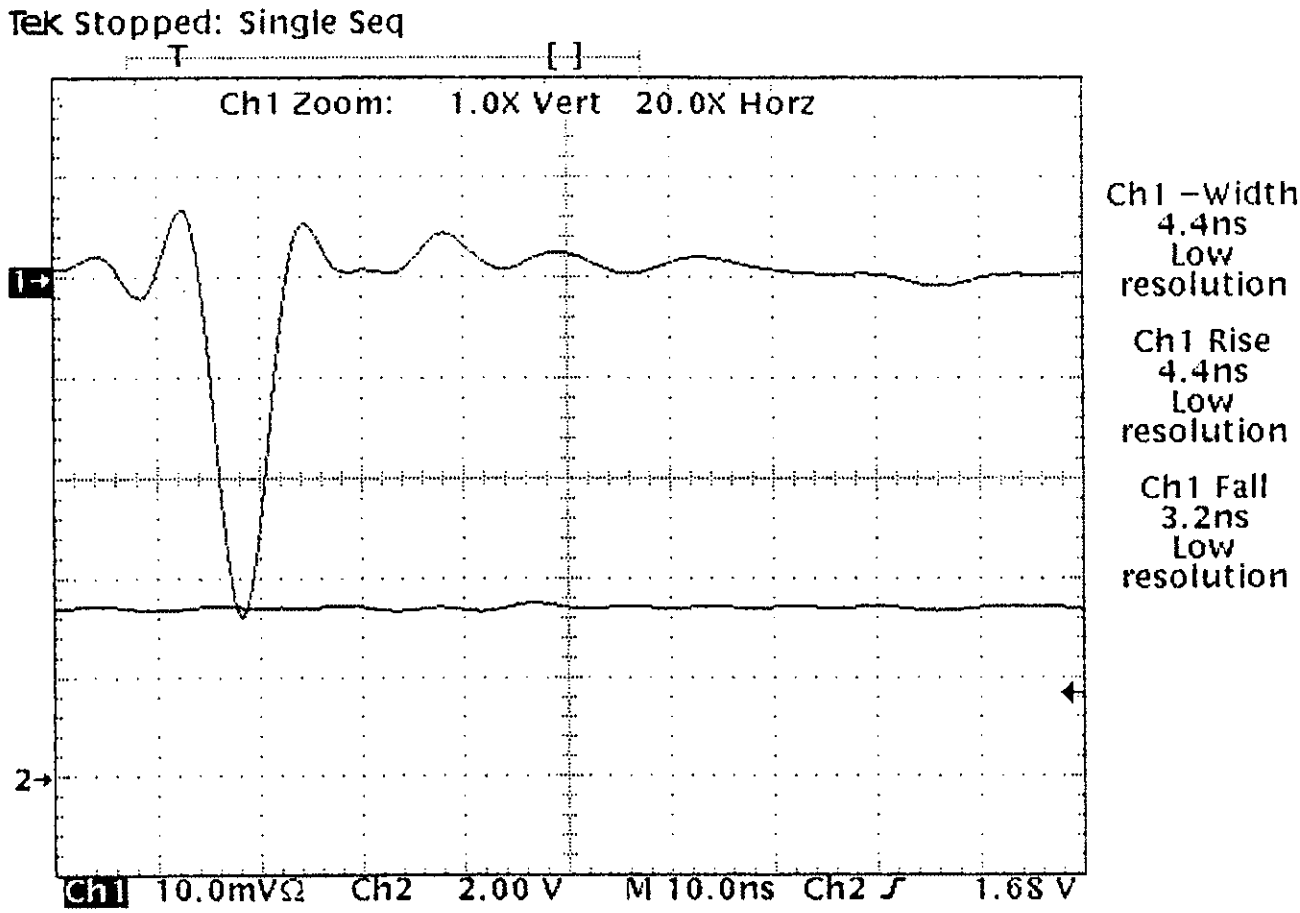

Figure B.1. Photomultiplier pulsed response without a snubbing circuit.

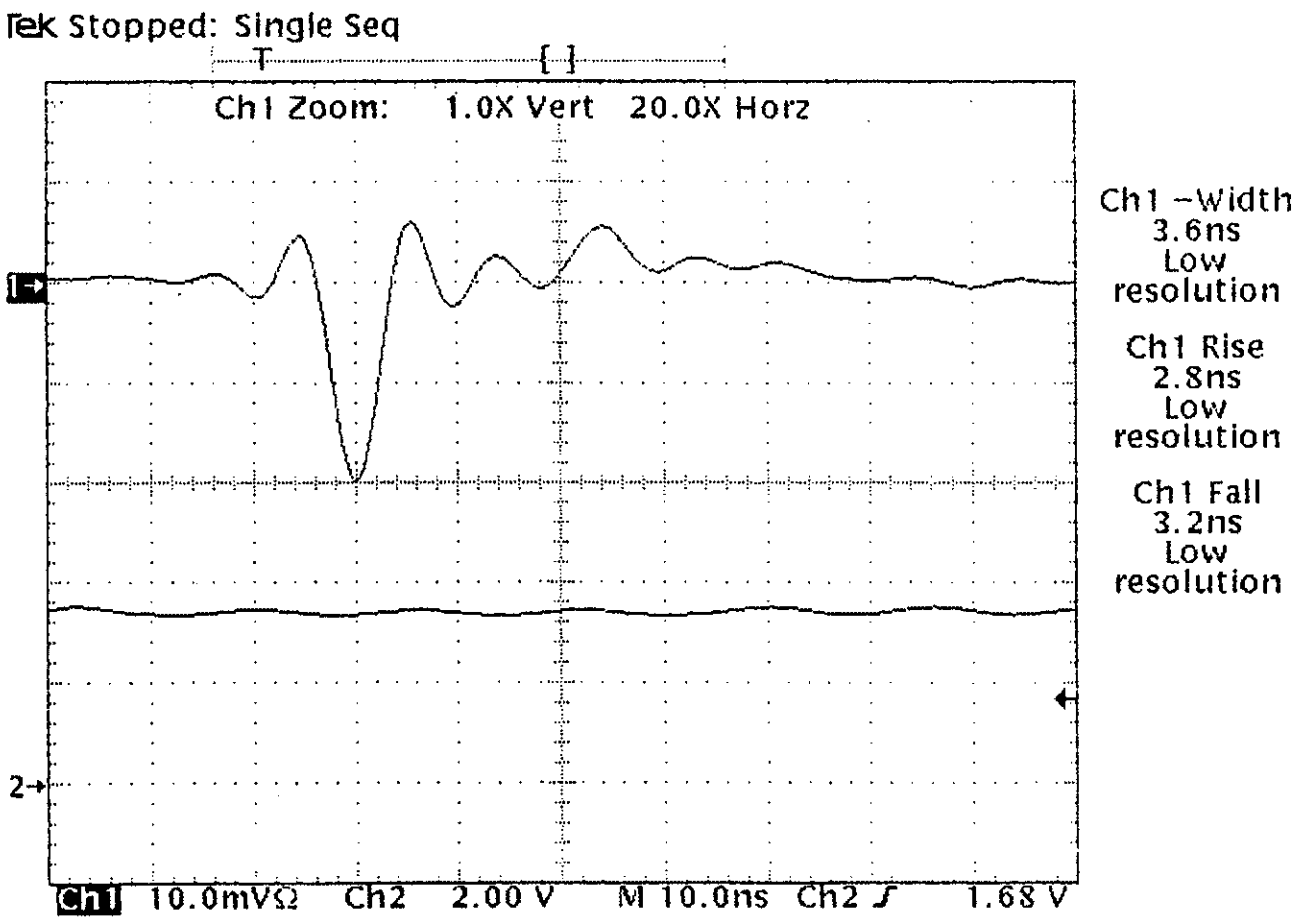

Figure B.2. Photomultiplier pulsed output using snubbing signal recovery.

APPENDIX C

OZONE DIAL TRANSMITTER AND SIGNAL PROCESSING SYSTEM

The DIAL measurement technique measures average ozone gas concentrations over a selected range interval by analyzing the difference in lidar backscatter signals produced by a laser signal tuned to the ozone gas molecular absorption line and another laser tuned off the absorption line [4,16,17]. The lidar laser signals are produced by an airborne DIAL system as shown in Figure C.1. Two frequency-doubled Nd:YAG lasers are used to pump two frequency-doubled tunable dye lasers. Each Nd:YAG produces a 1.6 J pulse at 532 nm and each dye laser produces 50 mJ per pulse at the 286 to 300 nm wavelengths. All four lasers are mounted together on a support structure that houses the laser power supplies, dual telescopes, and transmitting and receiving optics. The on- and off-wavelengths produced by the dye lasers yield sequential laser pulses controlled by the master control processor. An on- and off-line pulse separation of 300 μsec, at a 30 Hz laser repetition rate, ensures measurement by both wavelengths of the same atmospheric scattering volume [16]. The output beams are transmitted out 40 cm diameter quartz windows on the aircraft.

Nadir and zenith receiver systems consist of a 36 cm diameter telescope with dichroic optics that collect the received DIAL signals and direct them onto the appropriate

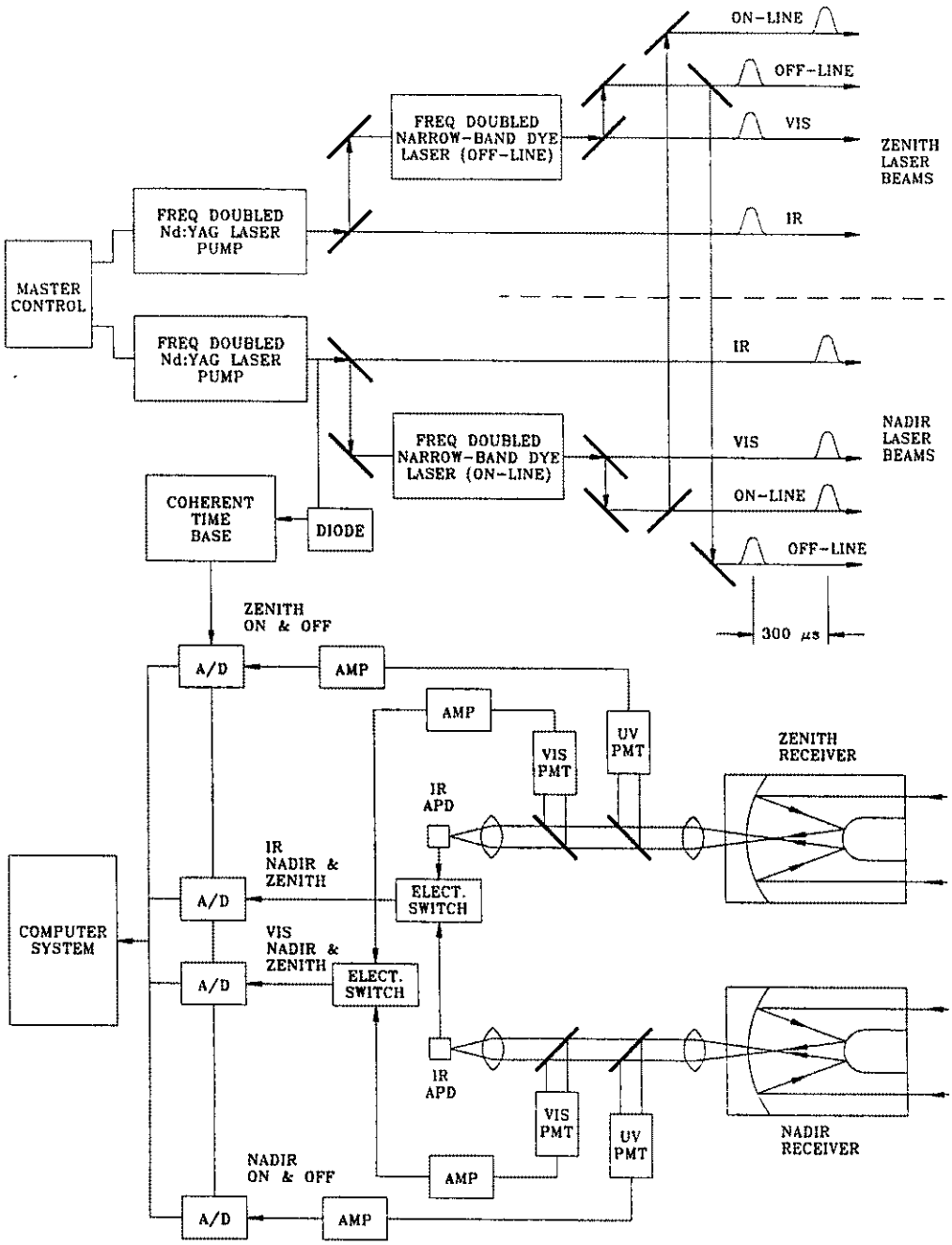

Figure C.1. Ozone DIAL transmitter, detector, and signal processing system [21].

detectors. Each analog signal is amplified at least 10 times and digitized by 12-bit transient digitizers, at a 10 MHz conversion rate, sequentially digitizing the on- and off-line ozone return signals [17]. Ozone concentrations can be calculated simultaneously in real time. The output can be displayed on a video screen or plotted in color for inflight analysis. The photon counting system was incorporated into the receiver ultraviolet channel using the zenith telescope. This was done in the laboratory to compare photon counting results with conventional analog detection for measuring improvements in the ozone detection range.

VITA

Bradley Allen Eccles

Bradley Allen Eccles was born in Phoenix, Arizona, in 1966. From 1989 through 1995 he served in the United States Navy as a Reactor Electrician aboard the nuclear aircraft carrier USS Enterprise (CVN65). He received the B.S.A.S.T.N.E.T. from Thomas Edison State College, Trenton, NJ and the B.S.E.E. (magna cum laude) from Old Dominion University, Norfolk, VA in 1995. His M.S.E.E. degree was supported, at Old Dominion University, through a grant funded by the National Aeronautics and Space Administration (NASA). From 1995 through 1997 he worked as a Graduate Research Assistant at NASA Langley Research Center where he conducted research and development of a photon counting system for ozone differential absorption lidar signal detection.

Mr. Eccles is a member of the Eta Kappa Nu Electrical Engineering Honor Society, Tau Beta Pi Engineering Honor Society, Golden Key Honor Society, and IEEE. He has earned the designation of Engineer-in-Training (EIT/FE).